Atmos. Chem. Phys., 21, 5615–5633, 2021
https://doi.org/10.5194/acp-21-5615-2021

Atmospheric Chemistry and Physics
Open Access
EGU

Drought-induced biomass burning as a source of black carbon to the central Himalaya since 1781 CE as reconstructed from the Dasuopu ice core

Joel D. Barker[1,2], **Susan Kaspari**[3], **Paolo Gabrielli**[1,2], **Anna Wegner**[2], **Emilie Beaudon**[2], **M. Roxana Sierra-Hernández**[2], **and Lonnie Thompson**[1,2]

[1]Byrd Polar and Climate Research Center, The Ohio State University, Columbus, OH 43210, USA
[2]School of Earth Sciences, The Ohio State University, Columbus, OH 43210, USA
[3]Department of Geological Sciences, Central Washington University, Ellensburg, WA 98926, USA

Correspondence: Joel D. Barker (barke269@umn.edu) and Paolo Gabrielli (gabrielli.1@osu.edu)

Received: 8 October 2020 – Discussion started: 20 October 2020
Revised: 19 February 2021 – Accepted: 27 February 2021 – Published: 13 April 2021

Abstract. Himalayan glaciers are melting due to atmospheric warming, with the potential to limit access to water for more than 25 % of the global population that resides in these glacier meltwater catchments. Black carbon has been implicated as a factor that is contributing to Himalayan glacier melt, but its sources and mechanisms of delivery to the Himalayas remain controversial. Here, we provide a 211-year ice core record spanning 1781–1992 CE for refractory black carbon (rBC) deposition from the Dasuopu glacier ice core that has to date provided the highest-elevation ice core record (7200 m). We report an average rBC concentration of $1.5\,\mu g\,L^{-1}$ (SD = 5.0, $n = 1628$) over the 211-year period. An increase in the frequency and magnitude of rBC deposition occurs after 1877 CE, accompanied by decreased snow accumulation associated with a shift in the North Atlantic Oscillation Index to a positive phase. Typically, rBC is deposited onto Dasuopu glacier during the non-monsoon season, and short-lived increases in rBC concentration are associated with periods of drought within neighboring regions in northwestern India, Afghanistan, and Pakistan. Using a combination of spectral and back-trajectory analyses, as well as a comparison with a concurrent analysis of trace metals at equivalent depths in the same ice core, we show that biomass burning resulting from dry conditions is a source of rBC to the central Himalaya and is responsible for deposition that is up to 60 times higher than the average rBC concentration over the time period analyzed. We suggest that biomass burning is a significant source of rBC to the central Himalaya and that the rBC record can be used to identify periods of drought in nearby regions that are upwind of Dasuopu glacier.

1 Introduction

Although the rate and extent of glacier melt differ geographically, the overall trend of glacier mass loss globally, particularly in mountain glaciers, is well documented (IPCC, 2013). While warming summer temperatures resulting in increased glacier mass loss (e.g., Gregory and Oerlemans, 1998) and decreasing precipitation as snow (Raper and Braithwaite, 2006) are important factors contributing to glacier mass wastage globally, the deposition of atmospheric aerosols that darken the glacier surface also contributes to melt (Flanner et al., 2007; Xu et al., 2009, 2012), particularly in proximity to aerosol emission sources. The most efficient of these aerosols is black carbon (BC), which is produced by a variety of combustion processes (Bond et al., 2004, 2013), most commonly by the incomplete combustion of fossil fuels and biomass (Jacobson, 2004; Hammes et al., 2007). BC is also the dominant absorber of visible light in the atmosphere (Lindberg et al., 1999) and exerts a positive radiative forcing globally, second only to CO_2 ($+1.1$ and $+1.6\,W\,m^{-2}$, respectively; Ramanathan and Carmichael, 2008). BC continues to absorb radiation upon deposition from the atmosphere onto glacier surfaces, reducing ice and snow albedo, which leads to melt

(Hansen and Nazarenko, 2004; Forster et al., 2007; Xu et al., 2009; Doherty et al., 2013).

A significant source of BC emitted to the atmosphere results from anthropogenic activity (Ramanathan and Carmichael, 2008; Bond et al., 2013). The BC flux to the atmosphere has increased by a factor of 2.5 since the Industrial Revolution, resulting in an increase in the global atmospheric BC burden by a factor of 2.5–3 (Lee et al., 2013). BC's relatively short atmospheric residence time influences its distribution globally, with the highest concentrations being proximal to BC emission sources (Bond et al., 2007, 2013; Xu et al., 2009). Asian regions surrounding the Himalaya are major sources of atmospheric BC (Novakov et al., 2003; Bond et al., 2007, 2013; Ramanathan et al., 2007), and southern Himalayan glaciers are particularly influenced by BC emissions from India (Kopacz et al., 2011; Gertler et al., 2016) and more local emission sources that may add to the broader-scale regional flux (Kaspari et al., 2011).

Atmospheric aerosols, including BC, are warming the cryosphere, accelerating snowmelt in the western Tibetan Plateau and Himalayas (Lau and Kim, 2010), and altering the regional hydrologic cycle (Immerzeel et al., 2010). This is a concern because Hindu Kush Himalayan (HKH) glacier melt affects water security, particularly during the early monsoon and post-monsoon season (Hill et al., 2020), for densely populated regions of Southeast Asia. Meltwater from HKH glaciers is the source of 10 major rivers that provide water for irrigation, hydropower, and ecosystem services for two billion people across Asia (Scott et al., 2019); this is over 25 % of the global population.

Research into BC's interaction with the HKH cryosphere has increased in recent years. Several studies have documented the magnitude and timing of BC deposition using short-term BC records preserved in surface snow that span 1–2 years (e.g., Xu et al., 2009; Ming et al., 2008, 2012; Kaspari et al., 2014; Zhang et al., 2018; Thind et al., 2019). More recently, continuous surface measurements of near-surface aerosols, including BC, have been reported for the HKH region (e.g., Marinoni et al., 2010; Bonasoni et al., 2010; Cao et al., 2010; Babu et al., 2011; Chaubey et al., 2011; Marinoni et al., 2013; Niu et al., 2017; Negi et al., 2019). While useful for tracking the evolution of atmospheric BC at high temporal resolution, these studies do not provide a longer-term historical context against which current levels of BC can be compared. Records of BC deposition preserved in ice cores are useful as longer-term environmental archives for reconstructing atmospheric aerosol composition that span decades (Liu et al., 2008; Ming et al., 2008; Ginot et al., 2014). In the HKH region, these archives are essential for identifying trends in BC deposition onto HKH glaciers in response to increasing BC emissions in surrounding regions. For example, Ming et al. (2008) report an increasing trend in BC deposition onto East Rongbuk glacier (Mt. Everest; 6500 m a.s.l.) during a 10-year period beginning in 1965 and then another increase beginning in 1995 to the end of the record in 2001. Xu et al. (2009) report a period of relatively high concentrations in the 1950s and 1960s in four Himalayan and Tibetan Plateau glaciers (Muztagh Ata, Guoqu glacier, Noijin Kangsang glacier, East Rongbuk glacier, and Tanggula glacier) and suggest a European source of BC to these sites. They also note an increase in BC on the easternmost site (Zuoqiupu glacier) beginning in the 1990s and suggest an Indian source of BC for the region. Similarly, Liu et al. (2008) report high elemental carbon at Muztagh Ata from 1955–1965. Ginot et al. (2014) report BC concentrations at Mera glacier from 1999–2010 and suggest that variations in BC over this period respond primarily to monsoonal rather than anthropogenic forcing.

Kaspari et al. (2011) were the first to present a BC record that extended back to the pre-industrial period (1860–2000) in an ice core from East Rongbuk glacier (6518 m a.s.l.) and reported a threefold increase in BC deposition since 1975, indicating that anthropogenic BC is contributing to the BC flux to the southern Himalaya. Jenkins et al. (2016) report an increase in BC deposition in the central Tibetan Plateau beginning in 1975 from the Guoqu glacier ice core record spanning 1843–1982. These deep ice core records are valuable for evaluating long-term trends in BC spanning the Industrial Revolution to the present and the concomitant increase in anthropogenically sourced BC emissions. Additional ice-core-derived BC records that span the period of industrialization in Asia are required to corroborate existing historical records of BC deposition onto HKH glaciers and to establish a regional baseline record for BC fluxes in the region. These records are currently lacking for the HKH and are essential for identifying regional-scale trends in BC deposition.

The highest-elevation ice core record ever obtained is the Dasuopu ice core (C3; Thompson et al., 2000), which was retrieved from the Dasuopu glacier in the central Himalaya (28.38° N, 85.72° E; Fig. 1) in 1997 at an elevation of 7200 m a.s.l. Thompson et al. (2000) determined that monsoonal precipitation is responsible for the net accumulation of snow onto the glacier surface, of the order of 1000 mm water equivalent per year (in 1996), permitting an annually resolved environmental record spanning 1440–1997 CE (Thompson et al., 2000). The remote location and high elevation of the Dasuopu ice core drill site suggest that any local influence on the deposition of atmospheric aerosols onto the glacier surface is minimal and that accumulation is representative of mixed free tropospheric composition (Kumar et al., 2015). Evidence suggesting that the Dasuopu glacier differs from lower-elevation glaciers in the region with respect to seasonal meteorology supports the hypothesis that the flux of aerosols onto the glacier surface may be more representative of free tropospheric composition rather than being affected by local (valley-scale) meteorological conditions (Li et al., 2011). Generally, the lower limit of the free troposphere in the central Himalaya occurs at $\sim$ 2.5 in the winter and 3.3 km in the summer (Solanki and Singh, 2014).

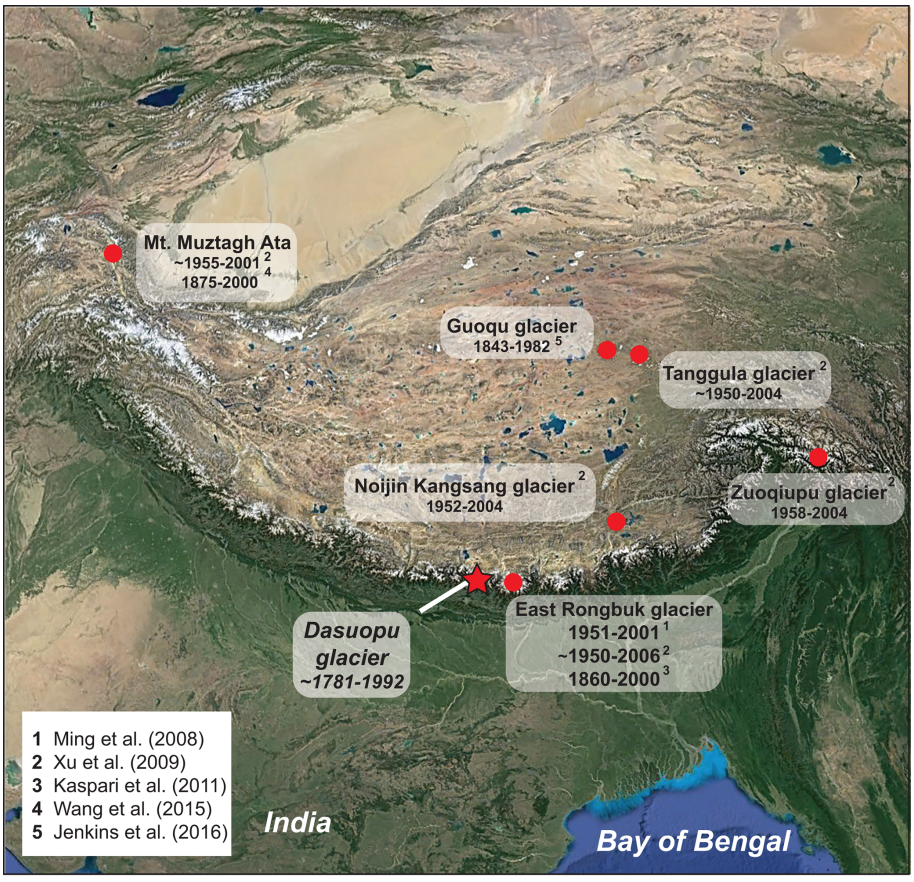

Figure 1. The location of Dasuopu glacier, Mt. Xixiabangma, and other ice cores that have provided a historical record of BC deposition in the region. The span of each BC record is indicated.

Here, we quantify refractory BC (rBC; a subset of the broader BC descriptor of carbonaceous particles that is specifically measured by laser-induced incandescence; Petzold et al., 2013; Lack et al., 2014) in a section of the Dasuopu ice core from 1781–1992 CE at annual to seasonal resolution in the glacier ice portion. We employ spectral analysis of the rBC ice core time series to identify trends in rBC deposited onto Dasuopu glacier across several temporal scales and to avoid "peak picking" that might lead to subjectively identifying episodes of increased rBC in the ice core time series. The rBC record is compared to trace element analysis of samples from equivalent depths along the same ice core, as described by Gabrielli et al. (2020), and an atmospheric back-trajectory analysis to elucidate the broader-scale trends of deposition and potential rBC sources to the southern Himalaya.

2 Methods

2.1 The Dasuopu ice core

Dasuopu glacier descends to the north from Mt. Xixiabangma in the central Himalaya (Fig. 1). The ice core examined here was drilled from the Dasuopu glacier surface to bedrock (145.4 m) with an electromechanical drill, without using drilling fluid, and provides a continuous record of deposition onto the glacier surface from 1010 to 1997 CE (Thompson et al. 2000). Here, we examine the upper section of the C3 ice core (hereafter referred to as the "Dasuopu core") from 8.4–120.3 m of depth from the surface, corresponding to the period 1781–1992 CE. Sections of the Dasuopu core outside this interval were not available for analysis. We use the Thompson et al. (2000) chronology that was established using $\delta^{18}O$, dust, and NO_3^- measurements, as well as annual layer counting confirmation using the location of the 1963 CE beta radioactivity peak from thermonuclear tests at a depth of 42.2 m to determine the core's age–depth relationship. Thompson et al. (2000) also used two major monsoon failures (1790–1796 and 1876–1877) as age–depth

benchmarks that are reflected in the dust and Cl^- records to validate the ice core dating chronology. The chronology is accurate to ±3 years (Thompson et al., 2000).

2.2 Sample preparation

A portion of the Dasuopu core has been housed in the Ice Core Storage Facility (Byrd Polar and Climate Research Center – BPCRC) at −30 °C since the original analysis by Thompson et al. (2000). The portion of the Dasuopu core analyzed here is characterized by consolidated firn from 8.4–56.4 m and glacier ice from 56.4–120.3 m of depth. Ice was sampled continuously (with the exception of intervals noted in Table S1 in the Supplement) in a cold room (−5 °C) at subannual resolution (2.5–10 cm sample interval) with a band saw along the length of the ice section. Each ice sample was divided in half to permit the analysis of BC and trace elements from identical depths throughout the core ($n = 1572$). Prior to rBC analysis, each ice sample was rinsed with type 1 Milli-Q (hereafter MQ) water at room temperature in a class 100 laboratory to remove any contaminants from the outer edges of the core, placed in a sealable polyethylene bag, and immediately stored frozen (−34 °C) to ensure that the sample did not melt prior to analysis.

Due to sample volume limitations resulting from previous studies of the Dasuopu core (e.g., Thompson et al., 2000; Davis et al., 2005), 52 firn samples (5.5–10 cm length) were collected at discontinuous intervals (where sufficient sample volume was available) from 8.4–56.4 m of depth in the cold room (−5 °C) using a band saw. The outer 2 cm of each sample ($n = 56$) was removed using clean stainless-steel knives (soaked in 2 N HNO_3^- and rinsed with MQ water) under laminar flow conditions in the cold room to remove surface contaminants. Clean firn samples were stored frozen (−30 °C) in double polypropylene bags until analysis.

2.3 BC analysis

The rBC was quantified by laser-induced incandescence using a single-particle soot photometer (SP2; Droplet Measurement Technologies, Longmont, USA; Schwarz et al., 2006; Wendl et al., 2014) at Central Washington University (Ellensburg, WA, USA). Frozen samples were melted at room temperature, transferred from storage bags into 50 mL polypropylene centrifuge tubes, and sonicated for 20 min immediately prior to analysis. Each liquid sample was stirred with a magnetic bar as water was routed into a CETAC U-5000AT+ ultrasonic nebulizer (Teledyne CETAC Technologies, Omaha, USA; ∼ 18 % nebulization efficiency at 220, 356, and 505 nm particle size; Menking, 2013; Wendl et al., 2014) using a peristaltic pump. The resultant aerosols flowed to the SP2 inlet at a known rate using carbon-free air carrier gas. The peak intensity of light emitted by an incandescing rBC particle is linearly proportional to its mass (Schwarz et al., 2006), and the SP2 detects this emitted light using the amplified output from two photodetectors (broadband and narrowband) to provide a detection range of ∼ 70–500 nm volume-equivalent diameter (VED; Kaspari et al., 2014). A five-point calibration curve (∼ 0.75–12.5 ppb) using Aquadag standards and MQ water was performed daily to correct for BC loss during nebulization (Wendl et al., 2014). MQ water was analyzed every five samples as a blank to monitor instrument baseline conditions. If the baseline was above background levels, then MQ water would be run through the system until stability was achieved. Baseline instability was not observed throughout the course of the analysis. The SP2 data output was processed using the PSI SP2 Toolkit version 4.100a (Paul Scherrer Institute, Switzerland) and the IGOR Pro software platform (WaveMetrics Inc., Portland, USA).

2.4 Spectral analysis

The record of rBC concentration with depth through the Dasuopu ice core provides a time series of rBC deposition onto Dasuopu glacier over time. The decomposition of the time series into time–frequency space using spectral analysis (wavelet analysis) permits the identification of dominant modes of variability and their variance with time (Torrence and Compo, 1998). Wavelet analysis is well suited to the analysis of time series data with a frequency and/or magnitude that is nonstationary through the signal (Debret et al., 2007). For example, wavelet analyses have been used to identify Himalayan climatic oscillations related to orbital forcing, Dansgaard–Oeschger cycles, and Heinrich events in the 1992 Guliya ice core (Yang et al., 2006). They have also been used to characterize the increased role of El Niño–Southern Oscillation (ENSO) climate forcing in Antarctic temperature since ∼ 1850 from ice core records from East and West Antarctica (Rahaman et al., 2019) as well as a switch from external forcing to internal forcing mechanisms on global climate during the mid-Holocene (Debret et al., 2009).

The ice core sampling strategy employed here may influence the results of the spectral analysis because the uppermost firn section was not sampled continuously and there are occasional sampling gaps in the glacier ice section (Table S1). The discontinuous sampling of the firn section likely resulted in an incomplete characterization of the rBC deposited onto the Dasuopu glacier since 1944 (56.4 m of depth). Further, the number of samples per year is not consistent throughout the record because of interannual differences in snow accumulation (Fig. S1 in the Supplement). It is important to note that the spectral analysis treats the rBC time series as a linear depth–time function. However, because the depth–time relationship in the ice core is not linear, data are treated here as a function of the sample number of progression with depth in the ice core, while the dates of the individual features detected relative to sample number are specified using the Thompson et al. (2000) depth–age model. Therefore, the spectral decomposition of the time series into time–

frequency space is achieved while minimizing the influence of data gaps and nonlinear accumulation rate.

The wavelet analysis of the Dasuopu rBC record was performed using the Wavelet Toolbox in MATLAB (version R2020a; MathWorks). A continuous 1-D wavelet transform was generated to identify modes of variability and the characteristics of that variability with time throughout the rBC record. The Mexican hat (or Rickler) mother wavelet was chosen because it is similar to the shape of the annual variability in the rBC concentration signal across the time series (Fig. S2 in the Supplement).

2.5 Trace element analysis

Trace element quantification at equivalent depths to the rBC was only possible for the glacier ice section of the Dasuopu ice core due to lack of sampling volume in the corresponding overlying firn sections. Trace element concentration was determined by inductively coupled plasma sector field mass spectrometry (ICP-SFMS) at BPCRC. A total of 23 trace elements were measured (Al, As, Ba, Bi, Cd, Co, Cr, Cs, Fe, Ga, Mg, Mn, Mo, Nb, Ni, Pb, Rb, Sb, Ti, Tl, U, V, and Zn) using methods described in Uglietti et al. (2014) and reported by Gabrielli et al. (2020). The trace element crustal enrichment factor (EF) is used to identify trace element contributions exceeding natural background levels and was calculated relative to Fe and elemental ratios of dust from the Tibetan Plateau following Gabrielli et al. (2020) as an additional variable to be compared with rBC.

2.6 Back-trajectory analysis

While the complex topography of the Himalayas affects local wind patterns, back-trajectory modeling permits the characterization of the broader regional catchment from which rBC may be derived. Atmospheric circulation capable of delivering rBC to Dasuopu glacier was identified using the Hybrid Single Particle Lagrangian Trajectory Model (HYSPLIT; NOAA Air Resources Laboratory). A 7 d back trajectory was chosen as a conservative estimate of rBC atmospheric residence time given the range reported in the literature (e.g., Ogren and Charlson, 1983; Reddy and Boucher, 2004, 2007; Samset et al., 2014; Lund et al., 2018). Back trajectories from the Dasuopu drill site were calculated at 6 h intervals from 1948–1991 for January (winter/non-monsoon) and July (summer/monsoon) using the NCEP/NCAR (National Centers for Environmental Prediction/National Center for Atmospheric Research) reanalysis from 1948 (the limit of the NCEP/NCAR dataset) to 1991.

3 Results

3.1 The rBC record

Figure 2a shows the 211-year rBC record from the Dasuopu ice core. The mean rBC concentration is $1.5\,\mu g\,L^{-1}$ (SD = 5.0, $n = 1628$) from 1781 (± 3 years) to 1992 CE. The mean rBC concentration in the glacier ice section from 1781 to 1944 and the discontinuously sampled firn section from 1944 to 1992 is 1.4 (SD = 4.4, $n = 1572$) and $6.0\,\mu g\,L^{-1}$ (SD = 13.5, $n = 52$), respectively. Note that the median values for the same time periods are less influenced by outliers with high concentrations (median 1781 to 1944 = 0.2, 1944 to 1992 = $0.6\,\mu g\,L^{-1}$). Even though the rBC concentration in the ice and firn described here is significantly different (two-tailed Mann–Whitney U test, $p < 0.05$), the effect of discontinuously sampling the firn section and its accurate characterization of rBC since 1944 is unknown. It is possible that the firn section is biased towards higher rBC concentrations because only 13 % (7 of 52) of the firn samples correspond to snow deposited during monsoon conditions, as indicated by depleted $\delta^{18}O$ (Fig. S4 in the Supplement), which is a period associated with lower atmospheric aerosol loading (Lelieveld et al., 2018). In general, increases in rBC concentration correspond to $\delta^{18}O$ enrichment (Fig. 3) and increased dust in glacier ice, indicating that higher rBC concentrations coincide with the non-monsoonal dry season (Figs. 3 and S4 for firn section; Kaspari et al., 2014). Occasional exceptions occur; for example, in 1824 CE a period of high rBC concentrations corresponds to a relatively low dust concentration and a low $\delta^{18}O$ value (Fig. 3a). The relationship between $\delta^{18}O$ enrichment and rBC over a broader and continuous time window is show in Fig. 3d. Here, an analysis of the magnitude-squared coherence between 1856 and 1943 at scales ranging from a single rBC measurement (period = 1) to 953 rBC measurements (period = 476 data points) shows high coherence at longer periods (> 256 data points) with no phase lag (as indicated by horizontal arrows oriented to the right) and strong coherence between 1878 and 1900 CE at a period of 24–120 data points ($\sim$ 2–10 years; 1 year = 12 data points; Fig. S1) with a lag in rBC of 0.25 for a cycle (as indicated by the vertical arrow) or 0.25–2.5 years (6–30 data points), suggesting that rBC increases at the end of the dry season during this period. There is also a band of strong coherence from 1910–1943 occurring with a periodicity of $\sim$ 15 years ($\sim 8\,points\,yr^{-1}$; Fig. S1) with no phase lag, suggesting that rBC concentrations reach their maximum at the peak of the dry season.

The smoothed (5-year median) rBC concentration and flux (the product of mean annual rBC concentration and snow accumulation) records show an increase beginning in $\sim$ 1870 and again in $\sim$ 1935 (Fig. 2a and b). The discontinuous firn section of the core has elevated concentrations during the late 1960s–1970s, consistent with observations from East Rong-

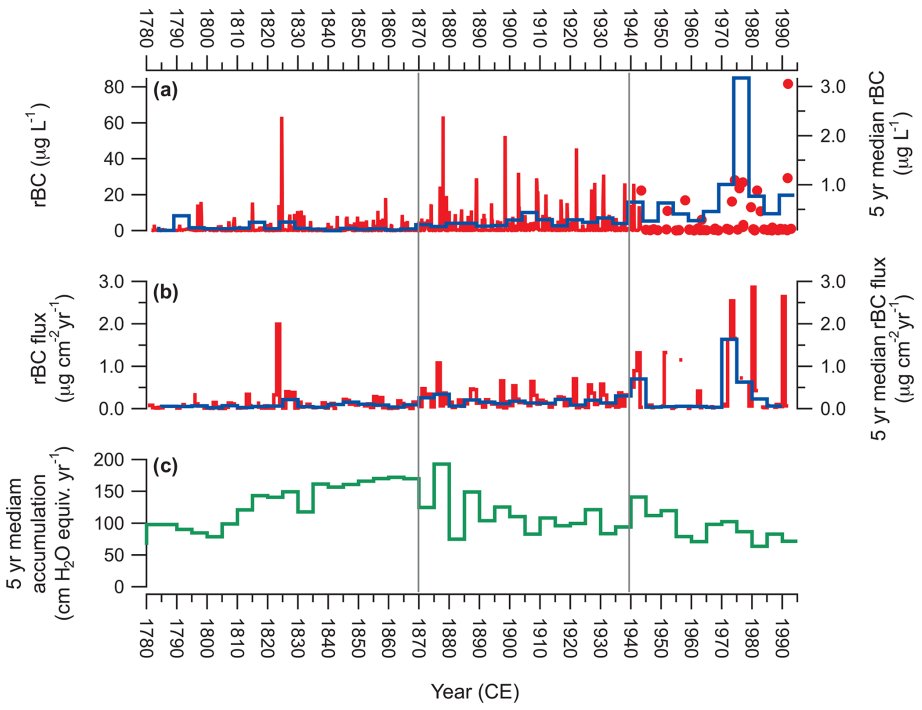

Figure 2. (a) The rBC record from the Dasuopu ice core (red). Red dots indicate discrete firn samples. The 5-year median is indicated (blue). **(b)** The rBC deposition flux onto Dasuopu glacier (red) with the 5-year median (blue). **(c)** The annual snow accumulation record for the Dasuopu ice core (Davis et al., 2005).

buk glacier by Ming et al. (2008) and Kaspari et al. (2011) and for Tanggula glacier by Xu et al. (2009).

3.2 Spectral analysis

We chose to examine three modes of variability within the spectral analysis (Fig. 4b), two of which correspond to North Atlantic sea surface temperature (SST), because of the important role of westerly atmospheric circulation in the Dasuopu region during the winter non-monsoonal season (Davis et al., 2005); the annual frequency is responsible for 90 % of the variance in the seasonal cycle of SST in the North Atlantic (Feliks et al., 2011) and ∼ 4.5-year variability that is the middle value of three modes of SST oscillation (3.7, 4.5, and 6.2 years; Feliks et al., 2011) in the Cape Hatteras region of the North Atlantic (44° N, 47° W). A third mode of variability (∼ 85 years) was chosen to identify longer-term variation in the rBC record.

The mode at $a = 6$ ($a = 0.5 \times$ frequency) indicates high-frequency and generally relatively low-amplitude variability in spectral coefficients (81 % of rBC concentrations are $< 1\,\mu g\,L^{-1}$) occurring at approximately annual (12 data points yr^{-1}; SD = 4.3, $n = 112$) resolution with isolated relatively higher-amplitude events dispersed throughout the record (Fig. 4c). The frequency of these higher-amplitude events increases from ∼ 1877 until 1992 CE (Fig. 4a and c).

The lower-frequency mode ($a = 27$; ∼ 4.5 years) captures periodic peaks in rBC concentrations centered at 1825, 1877, 1888, 1908, 1920, 1930, and 1977 CE if peaks that are > 25 % of the largest peak amplitude in the time series (1977 CE) are considered (Fig. 4d). Dips in the $a = 27$ spectral coefficients, indicating periods of low amplitude (defined here as > 25 % of the amplitude of the lowest dip at 1937 CE), occur at 1818, 1868, 1875, 1880–1884, 1893, 1914, 1924, and 1937 CE (Fig. 4d).

The $a = 512$ (∼ 85-year) mode identifies a shift from some samples with negative spectral coefficients (values below zero) to those with positive spectral coefficients at ∼ 1877 CE (Fig. 4e). All three modes identify a period early in the rBC record characterized as a quiescent period (1781–1877 CE) during which rBC concentrations do not exceed $19.3\,\mu g\,L^{-1}$ (mean = 0.8, SD = 3.0, $n = 880$), except for the isolated peak ($63.3\,\mu g\,L^{-1}$) at 1825 CE (Fig. 4a, c, and d). Prior to 1877 the rBC concentration in the ice core is significantly lower (Mann–Whitney U test, $p < 0.05$) and less variable (mean = 0.8, SD = 3.03, $n = 898$) than the post-1877 period (mean = 2.3, SD = 6.6, $n = 732$; Fig. 4). While the ∼ 85-year mode identifies a shift from negative to positive spectral coefficients in 1877, the 5-year median of the rBC record identifies an increase occurring at ∼ 1870. This suggests that the wavelet analysis may be sensitive to individual or tightly clustered peaks in the rBC record, such as those that occur between 1875 and 1880 (Figs. 3a and 4a).

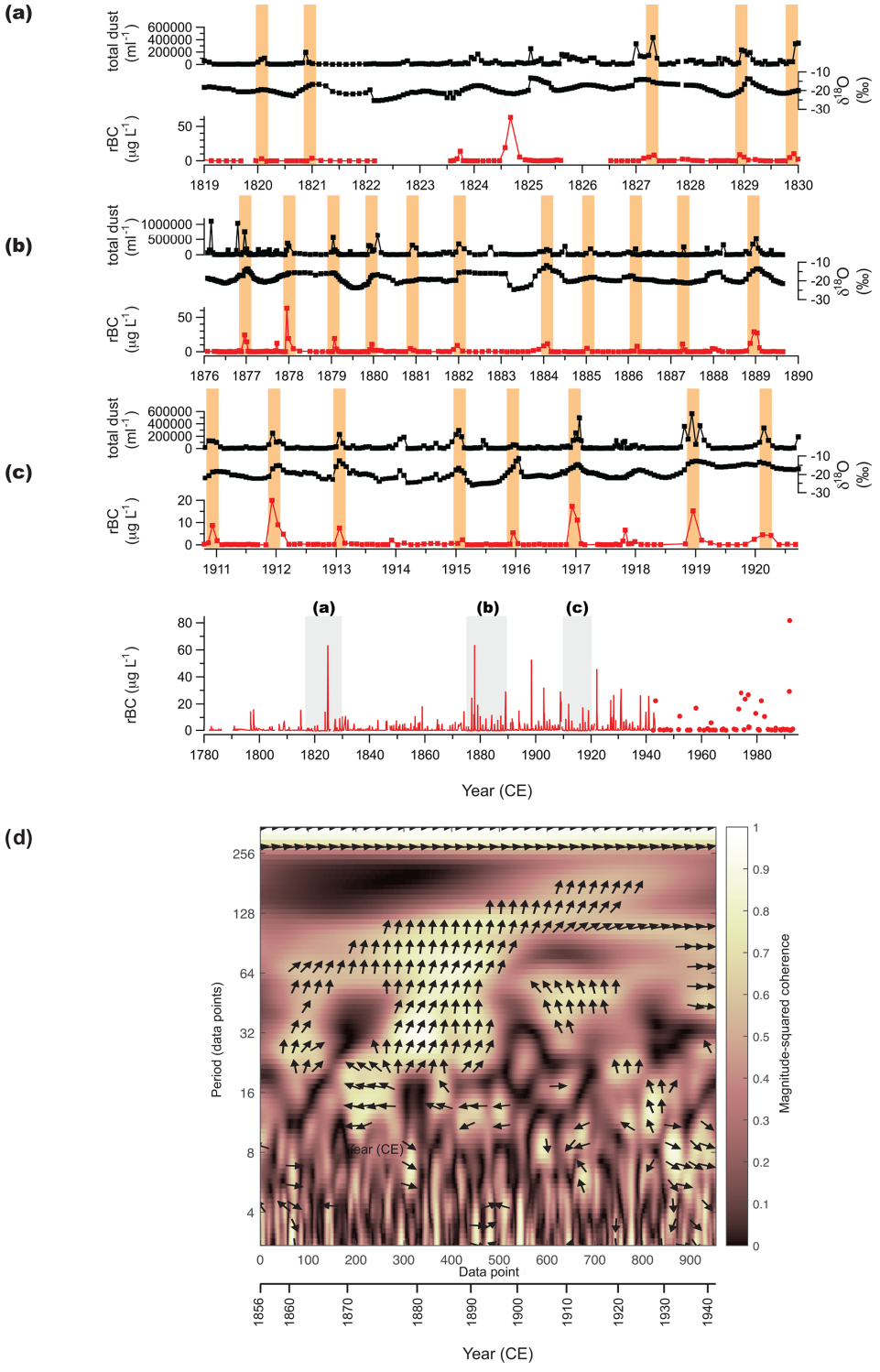

Figure 3. Peaks in the rBC record compared to the total dust and δ^{18}O records (Thompson et al., 2000) over three time intervals (**a**: 1819–1830, **b**: 1876–1890, **c**: 1911–1921 CE) in the Dasuopu ice core. Note that peaks in the rBC record are associated with depleted δ^{18}O and increased dust deposition. The spectral coherence between rBC and δ^{18}O between 1856 and 1943 CE **(d)** shows strong magnitude-squared coherence at a long period (∼ 21 years) with no phase lag (as shown by arrows oriented in radian space (i.e., the arrow oriented to the right indicates no phase lag; arrows oriented to the left indicate an antiphase relationship), strong magnitude-squared coherence between 2 and 10 years with a 0.5–2.5-year phase lag between 1878 and 1900 CE, and strong magnitude-squared coherence with no phase lag between 1910 and 1943 CE.

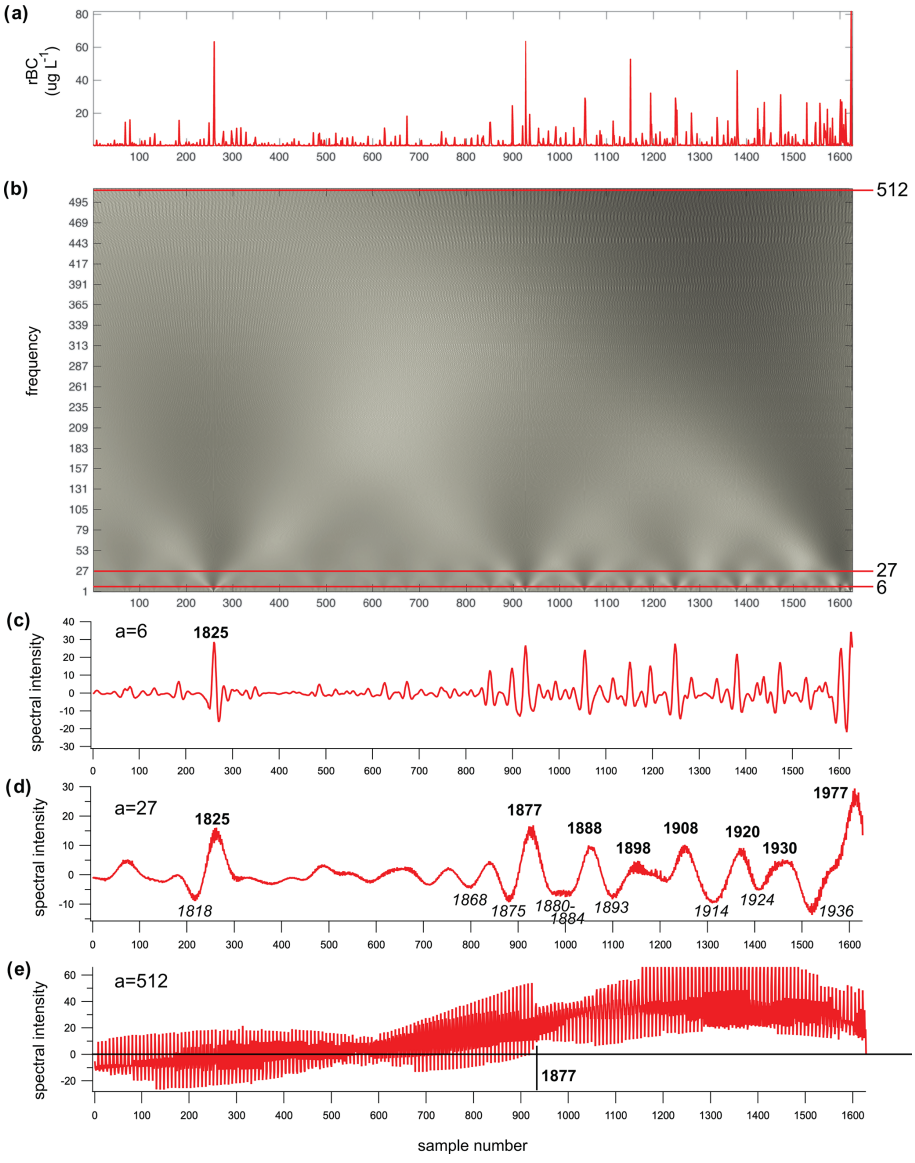

Figure 4. The spectral analysis of the Dasuopu rBC concentration record. Sample number 1 is located at the bottom of the ice core (1781 CE), and sample number 1628 is at the top of the firn section (1992 CE). **(a)** The rBC record plotted relative to sample number. **(b)** The spectral analysis showing variance across all frequency scales relative to sample number ranging from $a = 2$ to $a = 512$. Darker shades indicate relatively stronger (more positive) coherence between the wavelet and the rBC record, as indicated in the spectral coefficients. Panels **(c–e)** are the spectral coefficients relative to sample number for frequency scales $a = 6$, 27, and 512, respectively.

3.3 Comparison of the rBC record with the trace element record

When considering the full record ($n = 857$ to 916 depending on the element; Table 1), all of the trace element concentrations analyzed are significantly correlated with rBC (range of 0.15 for Zn at $n = 915$ to 0.27 for Rb at $n = 914$; Table 1; $\alpha = 0.01$). The Spearman correlation test is used instead of the Pearson correlation test because the rBC and trace element data are not normally distributed. If the low-rBC pre-1877 period, as indicated by the spectral analysis, is considered independently, then the correlation between trace elements and rBC is still statistically correlated (range of 0.26 for Zn at $n = 915$ to 0.44 for Mg and Mn at $n = 915$). In contrast, the post-1877 period shows a statistically insignificant slightly negative correlation between the trace elements and rBC ranging from -0.04 (Cs and Nb, $n = 913$ and 915, respectively) to -0.10 (Bi and Mn, $n = 857$ and 915, respectively).

The crustal enrichment factor (EF) for all of the trace elements was significantly weakly to moderately negatively correlated with rBC for all trace elements, ranging from -0.21

Table 1. The Spearman correlation coefficient (r_s, $\alpha = 0.01$) for trace elements and the trace element enrichment factor (EF) relative to rBC concentration throughout the Dasuopu ice core. Italics indicate a non-statistically significant r_s.

Trace element (n)	Total r_s	Pre-1877 r_s	Post-1877 r_s	EF total r_s	EF pre-1877 r_s	EF post-1877 r_s
Al (915)	0.22	0.40	*−0.08*	−0.45	−0.40	−0.55
As (914)	0.23	0.41	*−0.06*	−0.41	−0.41	−0.44
Ba (916)	0.26	0.43	*−0.07*	−0.24	−0.25	−0.28
Bi (857)	0.20	0.40	*−0.10*	−0.37	−0.33	−0.44
Cd (916)	0.23	0.37	*−0.07*	−0.50	−0.48	−0.62
Co (915)	0.23	0.41	*−0.09*	−0.38	−0.40	−0.42
Cr (915)	0.19	0.38	*−0.09*	−0.56	−0.53	−0.64
Cs (913)	0.25	0.41	*−0.04*	−0.39	−0.35	−0.48
Fe (915)	0.23	0.42	*−0.07*			
Ga (915)	0.22	0.39	*−0.07*	−0.57	−0.54	−0.68
Mg (915)	0.24	0.44	*−0.09*	−0.21	−0.20	−0.22
Mn (915)	0.24	0.44	*−0.10*	*0.02*	*−0.01*	*0.06*
Mo (915)	0.22	0.37	*−0.08*	−0.54	−0.52	−0.63
Nb (915)	0.21	0.36	*−0.04*	−0.48	−0.46	−0.59
Ni (915)	0.22	0.39	*−0.09*	−0.50	−0.50	−0.57
Pb (916)	0.23	0.40	*−0.08*	−0.31	−0.31	−0.35
Rb (914)	0.27	0.43	*−0.05*	−0.49	−0.47	−0.60
Sb (916)	0.19	0.38	*−0.07*	−0.56	−0.52	−0.65
Ti (914)	0.23	0.41	*−0.08*	−0.28	−0.25	−0.42
Tl (916)	0.24	0.42	*−0.08*	−0.52	−0.49	−0.62
U (916)	0.24	0.41	*−0.07*	−0.29	−0.29	−0.34
V (915)	0.24	0.40	*−0.07*	−0.52	−0.51	−0.63
Zn (915)	0.15	0.26	*−0.06*	−0.53	−0.52	−0.63

for Mg to −0.57 for Ga, except for Mn, which was insignificantly positively correlated (0.02). The trace element EFs were more negatively correlated with rBC during the post-1877 period than the pre-1877 period (excluding Mn because it was insignificantly correlated; SD = 0.14), although this difference is not statistically significant, with values $t(22) = 1.88$ and $p = 0.07$ ($p < 0.05$).

3.4 Back trajectory

Figure 5a shows the results of the July back trajectory: aerosols are primarily derived from areas to the southwest of the Dasuopu drill site, from the Arabian Sea, and across western and northern India during the monsoon. A secondary source is located to the west and draws atmospheric aerosols from the eastern Mediterranean Sea and Arabian Peninsula. January (non-monsoon) circulation is derived from the westerly circulation across northeastern Africa, central Europe, the Arabian Peninsula, and northwestern India (Fig. 5b).

4 Discussion

4.1 rBC concentrations

The mean rBC concentration in the Dasuopu ice core from 1781 to 1992 CE is 1.5 $\mu g\,L^{-1}$ (SD = 5.0, $n = 1628$); this is 6 times higher than the average rBC reported by Kaspari et al. (2011) for the period 1860–1992 and ∼ 2 times lower than BC reported by Ming et al. (2008) and Xu et al. (2009) for the East Rongbuk ice core record over similar time periods (Fig. 1). Note that while Kaspari et al. (2011) measured BC from the East Rongbuk core using the same incandescence method used here, samples were stored as liquid and measured concentrations are likely underestimated due to rBC particle adherence onto the walls of the storage container and/or agglomeration of BC particles above the detected particle size range (Wendl et al., 2014; Kaspari et al., 2014). In contrast, Ming et al. (2008) and Xu et al. (2009) measured BC concentration by thermo-optical methods, which may result in an overestimation of reported BC due to organic matter pyrolysis during analysis (Gilardoni and Fuzzi, 2017), and a larger fraction of the carbonaceous particles being classified as BC.

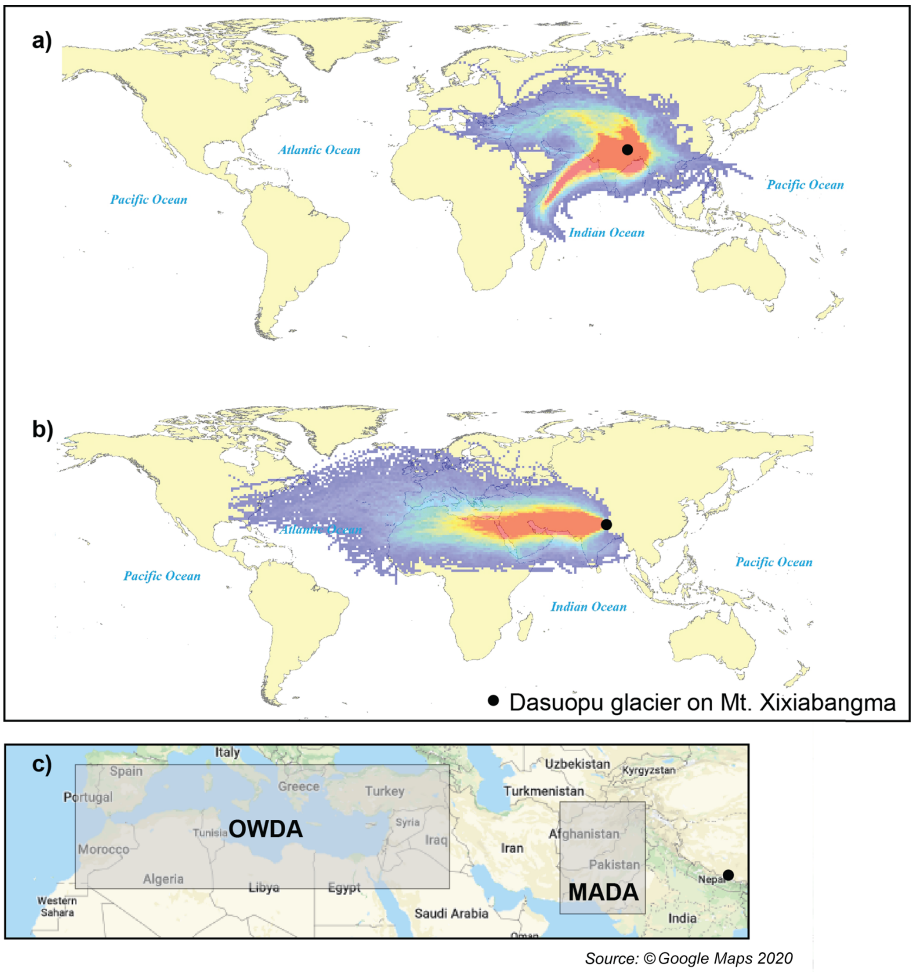

Figure 5. Frequency of back trajectories for air masses arriving at Mt. Xixiabangma in **(a)** July and **(b)** January. Red and blue indicate higher-frequency and lower-frequency air mass flow paths, respectively. The area included in the Old World Drought Atlas (OWDA; Cook et al., 2015) and the Monsoon Asia Drought Atlas (MADA; Cook et al., 2010) reconstructions is indicated **(c)**.

4.2 rBC seasonality

Seasonally, peaks in rBC concentration correspond to intervals of increased dust concentration and enriched $\delta^{18}O$ over the entire ice core record (see examples in Fig. 3), indicating that high BC concentrations are associated with the non-monsoonal season when drier westerly air masses dominate atmospheric circulation (Fig. 5). Weather station measurements and previous snow–ice studies in the region confirm that rBC concentrations are lower in near-surface air at the Nepal Climate Observatory-Pyramid (NCO-P; 5079 m a.s.l.) during the monsoon (Bonasoni et al., 2010; Marinoni et al., 2010, 2013) and higher during the pre-monsoon period (Babu et al., 2011; Nair et al., 2013; Ginot et al., 2014; Kaspari et al., 2014; Chen et al., 2018).

4.3 Temporal variations in high rBC concentrations and regional climate

The pre-1877 CE period differs from the post-1877 CE period in the frequency and amplitude of variability in rBC concentration (Figs. 2a and 4e). The high-rBC-concentration event in $\sim$ 1825 CE (Fig. 4c) occurs during an otherwise quiescent pre-1877 CE period coinciding with a time of severe regional moisture stress and droughts, as reflected in suppressed tree ring growth across Nepal, peaking in 1817 CE (Figs. 6 and 7 in Thapa et al., 2017). This period of abnormally dry conditions occurs after two large volcanic events: the Tambora eruption of 1815 (Stothers, 1984) and an eruption of unknown origin in 1809 CE (Cole-Dai et al., 2009). Anchukaitis et al. (2010) argue that major explosive eruptions in the tropics can disrupt the Asian monsoon system and result in drier conditions in central Asia for up to 8 years afterward. Dry conditions are typically associated with an increase in the frequency and severity of biomass burning in

Southeast Asia (Baker and Bunyavejchewin, 2009), and the association between dry conditions and increases in rBC concentration suggests that biomass burning may be a source of high-rBC-concentration events at Dasuopu glacier.

From ∼ 1877 CE until the end of the rBC record in 1992, rBC concentrations are significantly higher and their amplitude increases, as indicated by the shift from negative to positive spectral coefficients at $a = 512$ (Fig. 4e). This suggests a change in either the magnitude of rBC emission source(s) or in the atmospheric mechanism that delivers rBC to Dasuopu glacier after ∼ 1877 CE. The increase in rBC after ∼ 1877 corresponds to a decrease in snow accumulation onto Dasuopu glacier (Fig. 2c; Davis et al., 2005) and an increase in the rBC flux from the atmosphere beginning in ∼ 1880 (Fig. 2b). This decrease in snow accumulation has been linked to a strengthening of the Icelandic low-pressure system as temperatures in the Northern Hemisphere warmed at the termination of the Little Ice Age (LIA). This resulted in a shift in the North Atlantic Oscillation Index (NAO) from a negative mode to a positive mode, contributing less moisture to the southern Himalaya during winter (Davis et al., 2005). Less winter snow accumulation after ∼ 1877 would be associated with generally drier winter (non-monsoon) conditions when the rBC concentration is highest at Dasuopu glacier.

4.4 The influence of drought and biomass burning on the rBC record

Biomass burning and associated rBC emissions result from dry conditions and drought, which lowers the water table and dries out biomass fuel (Baker and Bunyavejchewin, 2009; Tosca et al., 2010). Further, aerosols produced during fires may contribute to a positive feedback cycle whereby smoke plume shading decreases sea surface temperature, while increased concentrations of atmospheric BC warm and stabilize the troposphere, suppressing convection and precipitation and intensifying drought conditions on land (Tosca et al., 2010). High BC aerosol levels in ambient air corresponding to agricultural burning beginning in late April and forest fire activity during the non-monsoon season were reported by Negi et al. (2019) from ambient air measurements at Chirbasa, India (Gangotri glacier valley) during 2016. The spectral coefficients calculated here identify trends in the rBC concentration on Dasuopu glacier and can be compared to regional rainfall data from a network of rain gauge stations that are distributed across India to identify periods of dryness (e.g., Parthasarathy et al. 1987) associated with higher rBC concentrations.

Continuous regional instrumental rainfall records within the atmospheric catchment for atmospheric aerosols at Dasuopu glacier prior to the early 1900s CE are rare, and biomass burning records are nonexistent. However, continuous tree-ring-based reconstructions of precipitation conditions for Europe, North Africa, and the Middle East are provided by the Old World Drought Atlas (OWDA; Cook et al., 2015) and include areas identified by the back-trajectory analysis as being potential source regions for rBC to Dasuopu glacier (Fig. 5b). The Monsoon Asia Drought Atlas (MADA; Cook et al., 2010) provides a similar dataset for regions in East Asia, including Pakistan and Afghanistan, which may contribute rBC on Dasuopu glacier (Fig. 5b). An instrumental record for both the OWDA and MADA begins in 1901 (Fig. 6). Comparing the peaks in rBC concentration identified by the spectral coefficients ($a = 27$, ∼ 4.5-year frequency) centered at 1825, 1877, 1888, 1898, 1908, 1920, 1930, and 1977 CE (Fig. 4d) to the reconstructed and instrumental self-calibrating Palmer Drought Severity Index (scPDSI) for the summer season (positive and negative scPDSI indicate wet and dry conditions, respectively; Fig. 6), it is possible to identify periods of dryness that might contribute to the production of rBC by biomass burning.

The rBC wavelet coefficient peaks in 1825 and 1877 CE occur at the end of a decade-long period of negative scPDSI in the OWDA and MADA reconstructions, respectively (Fig. 6). Similarly, 1888, 1898, and 1930 follow years of negative scPDSI in either the OWDA or MADA reconstructions, indicating periods of dryness preceding episodes of elevated rBC concentration at Dasuopu glacier (Fig. 6). The 1908 and 1920 CE peaks do not follow periods of negative scPDSI in the OWDA or MADA reconstructions, but they follow periods of negative scPDSI in the MADA instrumental record (Fig. 6), indicating that dryness is associated with these rBC concentration peaks as well. The peak centered at 1977 CE follows periods of positive scPDSI in the OWDA and MADA reconstructions and instrumental records. It does not appear to be related to abnormally dry conditions and may indicate an unidentified source of rBC. Conversely, dips in the spectral coefficients at a ∼ 4.5-year frequency ($a = 27$) indicate periods of low rBC concentration occurring at 1818, 1868, 1875, 1880-1884, 1893, 1914, 1924, and 1936 CE. With the exception of the dip centered at 1875 and 1936 CE, dips in the spectral coefficient record follow periods of positive scPDSI in either the OWDA and MADA tree ring reconstruction or both. While dips centered at 1914 and 1924 CE follow periods of positive scPDSI in both the OWDA and MADA instrumental record, 1936 CE follows a period of positive scPDSI in the MADA instrumental record only (Fig. 6).

In addition to the scPDSI from the OWDA and MADA tree ring reconstructions and the instrumental record (since 1900 CE), an independent historical record for rainfall is available for India that was compiled by Mooley et al. (1981) and has since been reported in terms of drought and flood severity by Parthasarathy et al. (1987; Supplement Table S1a and b). As mentioned, several periods of high rBC concentration are identified by the spectral coefficients at $a = 27$ (∼ 4.5-year frequency) centered at 1825, 1877, 1888, 1898, 1908, 1920, 1930, and 1977 CE (Fig. 4d). These periods of high rBC concentration coincide with periods of drought reported for India, particularly in western and northwestern meteorological subdivisions (Parthasarathy et al., 1987),

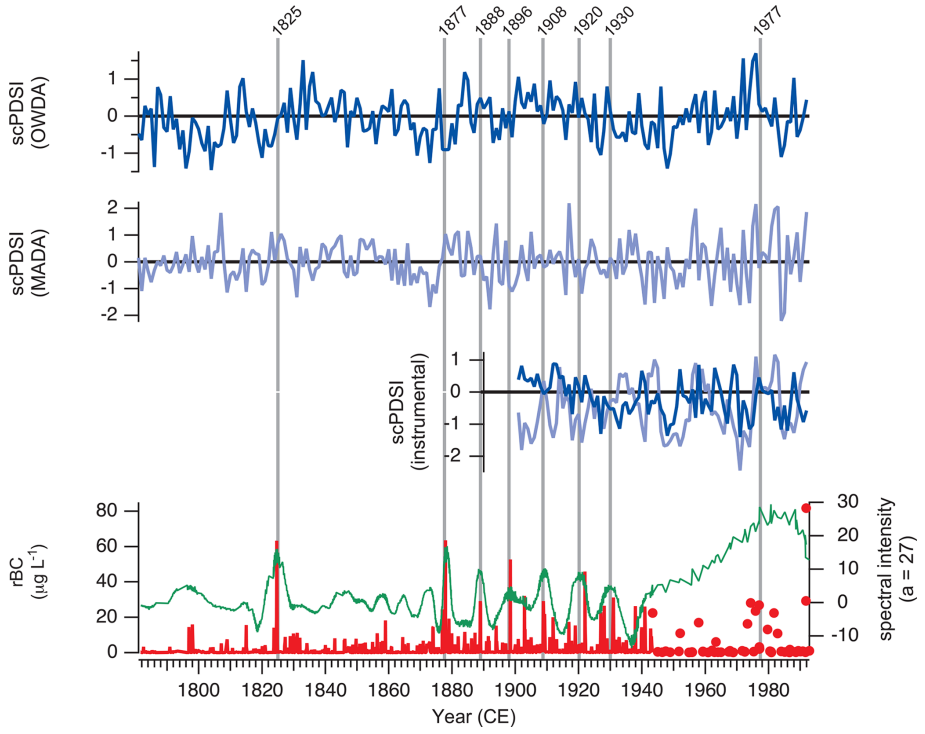

Figure 6. The Dasuopu rBC record (in red) compared to regional reconstructed and instrumental climate records from the Old World Drought Atlas (OWDA; dark blue) and the Monsoon Asia Drought Atlas (MADA; light blue). Note the correspondence between a negative self-calibrating Palmer Drought Severity Index (scPDSI) and periods of high rBC deposition. Data for both the reconstructed and instrumental climate records are obtained from the OWDA (drought.memphis.edu/OWDA/) and MADA (drought.memphis.edu/MADA).

within the ±3-year dating error of the ice core chronology (Fig. 7; Fig. S3a in the Supplement). For example, from 1876–1878, India experienced widespread moderate to severe drought conditions (Parthasarathy et al., 1987; Fig. 7a) and soil moisture deficits (Mishra et al., 2019) that resulted in the "Madras famine" (Cook et al., 2010; Mishra et al., 2019). In 1888 (and 1891, which is within the ±3-year ice core dating uncertainty), regions in western and northwestern India experienced moderate and severe drought conditions (Fig. 7b). In 1899 (corresponding to 1898 in the rBC record, ±3 years), northwestern and western meteorological subdivisions (among others) experienced severe drought, while moderate drought was experienced by most of India (Fig. 7c), resulting in famine that affected 59.5 million people (Mishra et al., 2019). In 1911 (1908 ± 3 years) there was extreme drought reported in the northwest and moderate drought reported in the north-central and southwestern meteorological districts (Fig. 7d). In 1918 (1920 ± 3 years), there was severe drought reported in the north and central-west and moderate drought reported throughout the southern and north-central regions of the continent (Fig. 7e). From 1927–1929 (1930 ± 3 years), moderate drought was reported in the northern region of India (Fig. 7f). Similar to observations from the OWDA and MADA comparisons, the ∼ 1977 period does not stand out in the climate record as being exceptional (Fig. S3), and it does not correspond to anomalously high rBC values (Fig. 2a), yet it corresponds to a period of highly positive spectral coefficients (Fig. 4c and d). Finite-length signal border effects (so-called edge effects) have been well documented, whereby a wavelet transform (such as that used here) yields abnormal coefficients as the wavelet extends into the "shoulder areas" of the record that do not have data (Su et al., 2011; Montanari et al., 2015). It is possible that the peak identified here at $a = 6$ and $a = 27$ is a result of wavelet transform edge effects. Alternatively, sources other than biomass burning that have not been identified here may contribute to the high rBC values observed in the Dasuopu ice core ∼ 1977 CE.

Dips in the $a = 27$ spectral coefficient record correspond to periods of flooding in India. For example, the trough at 1875 CE corresponds to reports of extreme flooding in the northwest and moderate flooding in western India (Fig. 8a). It should be noted that moderate drought was reported in the far west and south, but these conditions did not result in an rBC peak in the $a = 27$ coefficients (Fig. 4d). For the period ∼ 1880 to 1886 CE, severe and moderate flooding is reported in the west in 1884 CE, with moderate drought to the south and east that did not result in an rBC peak in the $a = 27$ coefficients (Fig. 8b). From 1880–1882 CE, the continent experienced relatively stable conditions, with moderate flood-

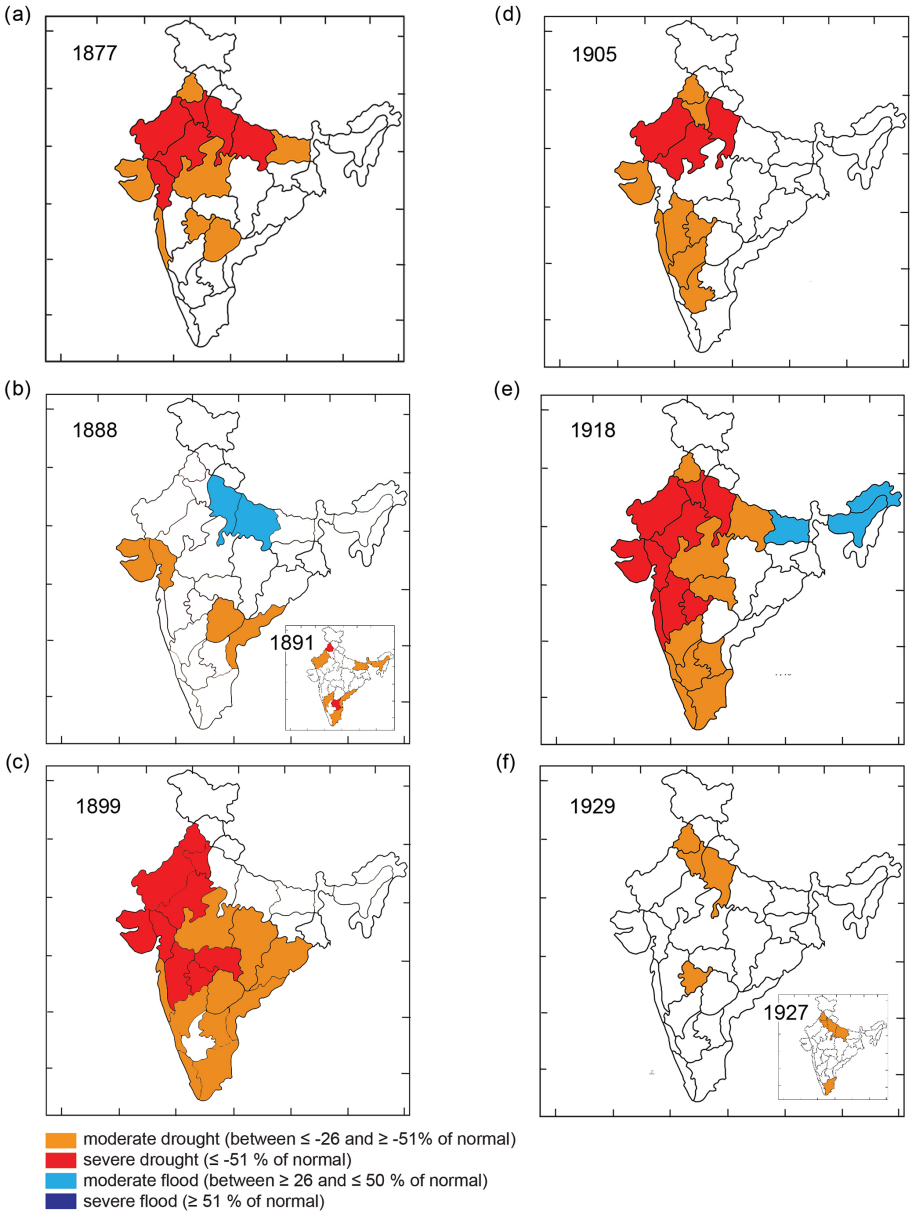

Figure 7. The distribution of meteorological subdivisions in NW India reporting drought during periods of high spectral intensity at $a = 27$ scale.

ing in some western and northwestern districts (Fig. S3). Western India experienced severe and moderate flooding in the west and northwest in 1893 (Fig. 8c), corresponding to a dip in the $a = 27$ coefficients (Fig. 4d). The years 1914 and 1917 (1914 ± 3 years), 1926 (1924 ± 3 years), and 1933 (1936 ± 3 years) all saw severe and/or moderate flooding in western meteorological districts, with no drought conditions reported in the rest of India, corresponding to dips in the $a = 27$ coefficients (Fig. 8d, e, and f, respectively).

4.5 rBC and trace metals

Recent work by Gabrielli et al. (2020) suggests that atmospheric trace metals preserved in the Dasuopu ice core, likely linked to the long-range transport of fine fly ash, are indicative of emissions from coal combustion and fires used to clear forested areas to the west of the Himalayas since the beginning of the Industrial Revolution (~ 1780 CE). Fly ash is composed of alumino-silicate and iron-rich by-products of coal combustion and biomass burning, and it is enriched in trace metals (Ross et al., 2002). Fly ash is not detected by the SP2 as configured here.

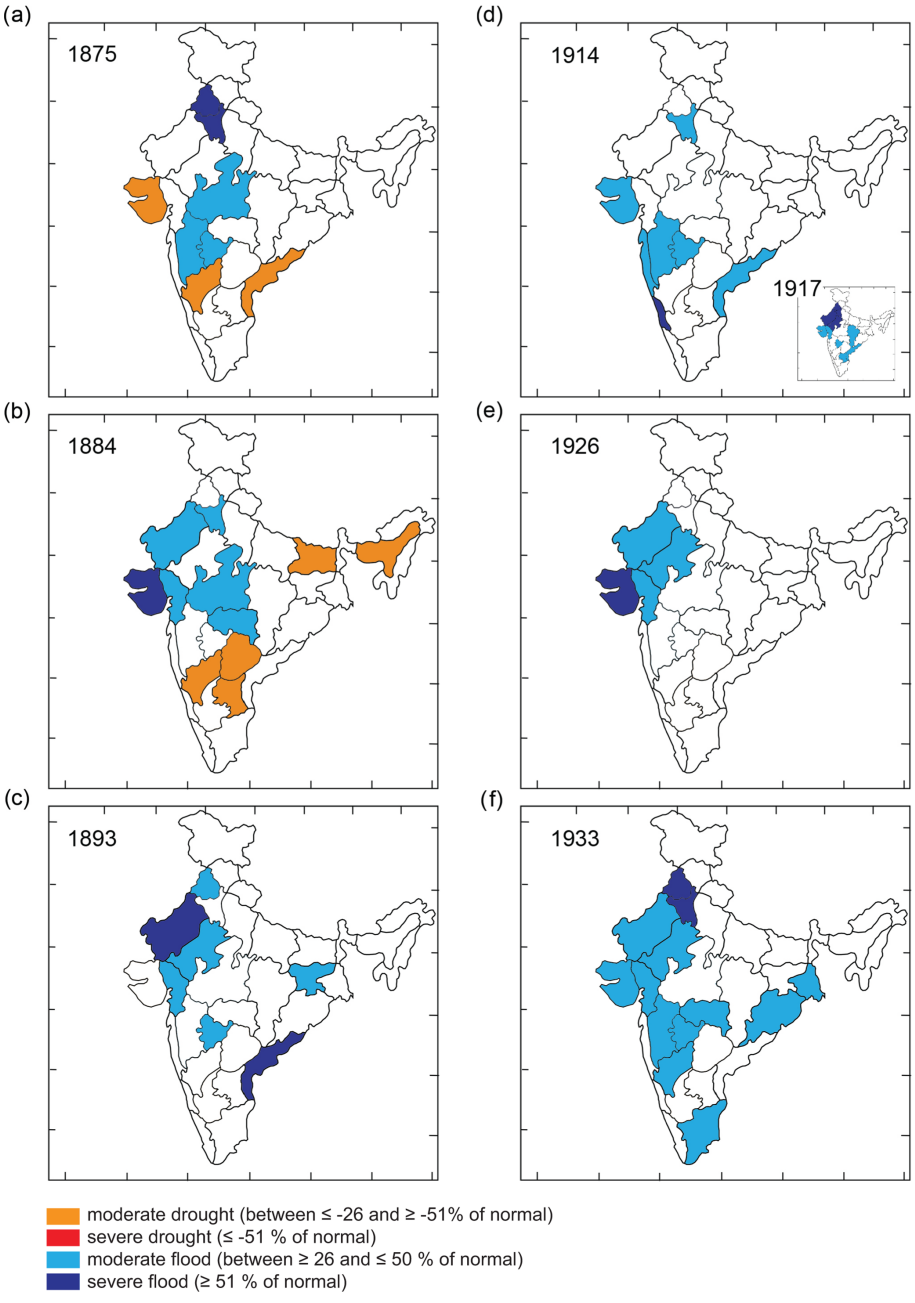

Figure 8. The distribution of meteorological subdivisions in NW India reporting flood conditions during periods of low spectral intensity at $a = 27$ scale.

We observe a general negative correlation between BC and the crustal enrichment factor (EF; indicative of element concentrations above the natural background derived from crustal material) of trace metals in the Dasuopu core, particularly after 1877 CE (Table 1) when rBC spectral coefficients are positive at $a = 512$ (Fig. 4e). This illustrates that the enrichment of the non-crustal fraction of trace metals (as indicated by a positive EF) and fly ash occurred out of phase from rBC.

Increases in the concentration of rBC resulting from biomass burning may be expected to correlate with trace elements associated with the biomass source material (K, Cl, Zn, and Br; Echalar et al., 1995). Of these, only Zn was analyzed here. The Zn concentration is only weakly correlated with rBC (0.15), although more strongly (0.26) in the pre-1877 period than in the post-1877 period (−0.06), and Zn's EF is moderately negatively correlated, particularly in the post-1877 period (−0.63). While the lack of correlation between potential biomass-burning-derived trace elements

such as Zn and rBC might suggest a non-biomass-burning source for rBC, one should be cautious in attributing specific trace elements to biomass burning events. For example, trace elements emitted during partial combustion can vary depending on fire intensity (flaming vs. smoldering), fuel source (savanna vs. forest) (Echalar et al., 1995), and size-dependent particle adhesion (Samsonov et al., 2012). Further, biomass burning remobilizes soil-derived particles, which would lower the individual trace element's EF (Gaudichet et al., 1995), causing a negative correlation between rBC and EFs. There is a statistically significant negative correlation with rBC for all of the trace element EFs (except for Mn), suggesting that rBC enrichment is not associated with non-crustal trace element enrichment, which is interpreted as an indicator of fly ash deposition (Gabrielli et al., 2020) that is enriched above the natural dust input. Of importance is that the discontinuous sampling of firn in the Dasuopu ice core record presented here does not capture a continuous record of rBC deposition during the post-1970s, which is a period when rBC is reported to have increased in the southern Himalaya (Kaspari et al., 2011) and Tibetan Plateau (Jenkins et al., 2016; Wang et al., 2015).

5 Conclusions

Here, we present the highest-elevation (7200 m a.s.l.) record of rBC ever reported. This record is unique in its high elevation and represents conditions in the free troposphere, away from local sources of BC. The Dasuopu record also contributes to the limited number of proxy records of BC in the HKH region where glacier melt, and therefore factors such as BC that affect glacier melt, influences the water security of one of the most densely populated regions of the planet. While the Dasuopu rBC record presented here is not well resolved during the period after the 1970s, the record does indicate elevated BC during 1970–1980, consistent with the Everest ice core BC record that shows elevated BC post-1970 (Kaspari et al., 2011).

The rBC concentration at the Dasuopu site is highest during the winter (non-monsoon) season when westerly circulation is dominant. Back-trajectory analyses indicate that this westerly circulation predominantly includes areas of western and northwestern India, Afghanistan, Pakistan, northern Africa, central Europe, and the Mediterranean. Dry conditions increase the production of rBC through biomass burning, and we suggest that regional biomass burning contributes to periods of high rBC deposition onto the Dasuopu glacier during periods of dryness as indicated by historical records of precipitation within the atmospheric catchment of Dasuopu glacier. The continuous historical record of precipitation for India, in particular, suggests an association between moderate to severe drought conditions in western and northwestern India and rBC concentration in the Dasuopu ice core. Upwind industrial sources of rBC, such as coal combustion, appear to be of minor influence during these periods of increased rBC deposition as indicated by the absence of correlation between rBC concentration in the Dasuopu core and the crustal enrichment of industrially sourced trace elements at equivalent depths in the ice core. It should be noted that the Dasuopu ice core rBC record is discontinuous during the period of increased regional industrial activity; thus, the available data cannot address the importance of this regional industrialization for rBC deposition onto Dasuopu glacier. Together, evidence presented here indicates that while rBC transport in the free troposphere is influenced by large-scale synoptic circulation, regional sources of rBC strongly influence rBC deposition onto Dasuopu glacier, particularly after $\sim$ 1877, and that the rBC record from Dasuopu glacier may provide a proxy record for drought and resultant biomass burning within its catchment of atmospheric circulation.

Data availability. The data presented in this work are archived at the National Oceanic and Atmospheric Administration World Data Service for Paleoclimatology at https://www.ncdc.noaa.gov/paleo/study/32952 (Barker, 2021).

Supplement. The supplement related to this article is available online at: https://doi.org/10.5194/acp-21-5615-2021-supplement.

Author contributions. JDB performed the sample preparation, BC analysis, and interpretation and was the primary author of the paper. SK assisted with the BC analysis and interpretation of the BC record. PG designed the overall project and performed the trace element analysis with AW. AW, EB, and MRS-H cut the samples from the ice core and performed the trace element analysis. LT retrieved the Dasuopu ice core. All authors contributed to paper preparation.

Competing interests. The authors declare that they have no conflict of interest.

Acknowledgements. This work was funded by the NSF Atmospheric Chemistry Program, the NSF-ESH program, The Ohio State University, the Ohio State Committee of Science and Technology, and the National Natural Science Foundation of China. We thank the many scientists, engineers, technicians, and graduate students from the Byrd Polar and Climate Research Center and the Lanzhou Institute of Glaciology and Geocryology (China) that contributed to the collection and previous analysis of the Dasuopu ice core. We are grateful to Julien Nicolas for performing the graphic display of the back trajectories. We thank two anonymous reviewers who provided input to greatly improve this paper.

Financial support. This research has been supported by the NSF Atmospheric Chemistry Program (grant no. 1149239).

Review statement. This paper was edited by Aurélien Dommergue and reviewed by two anonymous referees.

References

Anchukaitis, K. J., Buckley, B. M., Cook, E. R., D'Arrigo, R. D., and Ammann, C. M.: Influence of volcanic eruptions on the climate of the Asian monsoon region, Geophys. Res. Lett., 37, 1–5, https://doi.org/10.1029/2010GL044843, 2010.

Babu, S. S., Chaubey, J. P., Moorthy, K. K., Gogoi, M. M., Kompalli, K. K., Sreekanth, V., Bagare, S. P., Bhatt, B. C., Gaur, V. K., Prabhu, T. P., and Singh, N. S.: High altitude (∼ 4520 m amsl) measurements of black carbon aerosols over western trans-Himalayas: Seasonal heterogeneity and source apportionment, J. Geophys. Res.-Atmos., 116, D24201, https://doi.org/10.1029/2011JD016722, 2011.

Baker, P. J., and Bunyavejchewin, S.: Fire behavior and fire effects across the forest landscape of continental Southeast Asia, in: Tropical Fire Ecology, Springer Praxis Books, Springer, Berlin, Heidelberg, https://doi.org/10.1007/978-3-540-77381-8_11, 2009.

Barker, J. D.: Dasuopu, China 210 Year Ice Core Refractory Black Carbon Data, NOAA National Centers for Environmental Information, available at: https://www.ncdc.noaa.gov/paleo-search/study/32952, last access: 7 April 2021.

Bonasoni, P., Laj, P., Marinoni, A., Sprenger, M., Angelini, F., Arduini, J., Bonafè, U., Calzolari, F., Colombo, T., Decesari, S., Di Biagio, C., di Sarra, A. G., Evangelisti, F., Duchi, R., Facchini, MC., Fuzzi, S., Gobbi, G. P., Maione, M., Panday, A., Roccato, F., Sellegri, K., Venzac, H., Verza, GP., Villani, P., Vuillermoz, E., and Cristofanelli, P.: Atmospheric Brown Clouds in the Himalayas: first two years of continuous observations at the Nepal Climate Observatory-Pyramid (5079 m), Atmos. Chem. Phys., 10, 7515–7531, https://doi.org/10.5194/acp-10-7515-2010, 2010.

Bond, T. C., Streets, D. G., Yarber, K. F., Nelson, S. M., Woo, J.-H., and Klimont, Z.: A technology-based global inventory of black and organic carbon emissions from combustion, J. Geophys. Res.-Atmos., 109, D14, https://doi.org/10.1029/2003JD003697, 2004.

Bond, T. C., Bhardwaj, E., Dong, R., Jogani, R., Jung, S., Roden, C., Streets, D. G., and Trautmann, N. M.: Historical emissions of black and organic carbon aerosol from energy-related combustion, 1850-2000, Global Biogeochem. Cy., 21, GB2018, https://doi.org/10.1029/2006GB002840, 2007.

Bond, T. C., Doherty, S. J., Fahey, D. W., Forster, P. M., Bernsten, T., DeAngelo, B. J., Flanner, M. G., Ghan, S., Karcher, B., Koch, D., Kinne, S., Kondo, Y., Quinn, P. K., Sarofim, M. C., Schultz, M. G., Shulz, M., Venkataraman, C., Zhang, H., Zhang, S., Bellouin, N., Guttikunda, S. K., Hopke, P. K., Jaconson, M. Z., Kaiser, J. W., Klimont, Z., Lohmann, U., Schwarz, J. P., Shindell, D., Storelvmo, T., Warren, S. G., and Zender, C. S.: Bounding the role of black carbon in the climate system: A scientific assessment, J. Geophys. Res.-Atmos, 118, 5380–5552, https://doi.org/10.1002/jgrd.50171, 2013.

Cao, J., Tie, X., Xu, B., Zhao, Z., Zhu, C., Li, G., and Liu, S.: Measuring and modeling black carbon (BC) contamination in the SE Tibetan Plateau, J. Atmos. Chem., 67, 45–60, https://doi.org/10.1007/s10874-011-9202-5, 2010.

Chaubey, J. P., Babu, S. S., Gogoi, M. M., Kompalli, S. K., Sreekanth, V., Moorthy, K. K., and Prabhu, T. P.: Black carbon aerosol over a high altitude (∼ 4.52 km) station in Western Indian Himalayas, J. Inst. Eng., 8, 42–51, https://doi.org/10.3126/jie.v8i3.5930, 2011.

Chen, X., Kang, S., Cong, Z., Yang, J., and Ma, Y.: Concentration, temporal variation, and sources of black carbon in the Mt. Everest region retrieved by real-time observation and simulation, Atmos. Chem. Phys., 18, 12859–12875, https://doi.org/10.5194/acp-18-12859-2018, 2018.

Cole-Dai, J., Ferris, D., Lanciki, A., Savarino, J., Baroni, M., and Thiemens, M. H.: Cold decade (AD 1810–1819) caused by Tambora (1815) and another (1809) stratospheric volcanic eruption, Geophys. Res. Lett., 36, L22703, https://doi.org/10.1029/2009GL040882, 2009.

Cook, E. R., Anchukaitis, K. J., Buckley, B. M., D'Arrigo, R. D., Jacoby, G. C., and Wright, W. E.: Asian monsoon failure and megadrought during the last millennium, Science, 328, 486–489, https://doi.org/10.1126/science.1185188, 2010.

Cook, E. R., Seager, R., Kushnir, Y., Briffa, K. R., Buntgen, U., Frank, D., Krusic, P. J., Tegel, W., van der Schrier, G., Andreu-Hayles, L., Baillie, M., Baittinger, C., Bleicher, N., Bonde, N., Brown, D., Carrer, M., Cooper, R., Cufar, K., Dittmar, C., Esper, J., Griggs, C., Gunnarson, B., Gunther, B., Gutierrez, E., Haneca, K., Helama, S., Herzig, F., Heussner, K.-U., Hofmann, J., Janda, P., Kontic, R., Kose, N., Kynci, T., Levanic, T., Linderholm, H., Manning, S., Melvin, T. M., Miles, D., Neuwirth, B., Nicolussi, K., Nola, P., Panayotov, M., Popa, I., Rothe, A., Seftigen, K., Seim, A., Svarva, H., Svoboda, M., Thun, T., Timonen, M., Touchan, R., Trotsiuk, V., Trouet, V., Walder, F., Wazny, T., Wilson, R., and Zang, C.: Old world megadroughts and pluvials during the Common Era, Sci. Adv., 1, e1500561, https://doi.org/10.1126/sciadv.1500561, 2015.

Davis, M. E., Thompson, L. G., Yao, T., and Wang, N.: Forcing of the Asian monsoon on the Tibetan Plateau: Evidence from high-resolution ice core and tropical coral records, J. Geophys. Res., 110, D04101, https://doi.org/10.1029/2004JD004933, 2005.

Debret, M., Bout-Roumazeilles, V., Grousset, F., Desmet, M., McManus, J. F., Massei, N., Sebag, D., Petit, J.-R., Copard, Y., and Trentesaux, A.: The origin of the 1500-year climate cycles in Holocene North-Atlantic records, Clim. Past, 3, 569–575, https://doi.org/10.5194/cp-3-569-2007, 2007.

Debret, M., Sebag, D., Costra, X., Massei, N., Petit, J.-R., Chapron, E., and Bout-Roumazeilles, V.: Evidence from wavelet analysis for a mid-Holocene transition in global climate forcing, Quaternary Sci. Rev., 28, 2675–2688, https://doi.org/10.1016/j.quascirev.2009.06.005, 2009.

Doherty, S. J., Grenfell, T. C., Forsström, Hagg, D. L., Brandt, R. E., and Warren, S. G.: Observed vertical redistribution of black carbon and other insoluble light-absorbing particles in melting snow, J. Geophys. Res.-Atmos., 118, 5553–5569, https://doi.org/10.1002/jgrd.50235, 2013.

Echalar, F., Gaudichet, A., Cachier, H., and Artaxo, P.: Aerosol emissions by tropical forest and savanna biomass burning: characteristic trace elements and fluxes, Geophys. Res. Lett., 22, 3039–3042, https://doi.org/10.1029/95GL03170, 1995.

Feliks, Y., Ghil, M., and Robertson, A. W.: The atmospheric circulation over the North Atlantic as induced by the SST field, J. Clim., 24, 522–542, https://doi.org/10.1175/2010JCLI3859.1, 2011.

Flanner, M. G., Zender, C. S., Randerson, J. T., and Rasch, P. J.: Present day climate forcing and response from black carbon in snow, J. Geophys. Res., 112, D11202, https://doi.org/10.1029/2006JD008003, 2007.

Forster, P., Ramaswamy, V., Artaxo, P., Berntsen, T., Betts, R., D. W., Haywood, J., Lean, J., Lowe, D. C., Myhre, G., Nganga, J., Prinn, R., Raga, G., Schulz, M., and Van Dorland, R.: Changes in Atmospheric Constituents and in Radiative Forcing, in: Climate Change 2007: The Physical Science Basis. Contribution of Working Group I to the Fourth Assessment Report of the Intergovernmental Panel on Climate Change, edited by: Solomon, S., Qin, D., Manning, M., Chen, Z., Marquis, M., Averyt, K. B., Tignor, M., and Miller, H. L., Cambridge University Press, Cambridge, United Kingdom and New York, USA., 131–234, ISBN 978-0521-70596-7, 2007.

Gabrielli, P., Wegner, A., Sierra Hernández, R., Beaudon, E., Davis, M., Barker, J. D., and Thompson, L. G., Early contamination of the Himalayan atmosphere from coal combustion since the onset of the European Industrial Revolution (∼ 1780 A.D.), P. Natl. Acad. Sci. USA, 117, 3967–3973, https://doi.org/10.1073/pnas.1910485117, 2020.

Gaudichet, A., Echalar, F., Chatenet, B., Quisefit, J. P., and Malingre, G.: Trace elements in tropical African savanna biomass burning aerosols, J. Atmos. Chem., 22, 19–39, https://doi.org/10.1007/BF00708179, 1995.

Gertler, C. G., Puppala, S. P., Panday, A., Stumm, D., and Shea, J.: Black carbon and the Himalayan cryosphere: A review, Atmos. Environ., 125, 404–417, https://doi.org/10.1016/j.atmosenv.2015.08.078, 2016.

Gilardoni, S., and Fuzzi, S.: Chemical composition of aerosols of different origin, in: Atmosphereic Aerosols: Life Cycles and Effects of Air Quality and Climate, edited by: Tomasi, C., Fuzzi, S., and Kokhanovsky, A., Wiley-VCH Verlag GmbH & Co. KGaA, Weinheim, 183–221, https://doi.org/10.1002/9783527336449.ch4, 2017.

Ginot, P., Dumont, M., Lim, S., Patris, N., Taupin, J.-D., Wagnon, P., Gilbert, A., Arnaud, Y., Marinoni, A., Bonasoni, P., and Laj, P.: A 10 year record of black carbon and dust from a Mera Peak ice core (Nepal): variability and potential impact on melting of Himalayan glaciers, The Cryosphere, 8, 1479–1496, https://doi.org/10.5194/tc-8-1479-2014, 2014.

Gregory, J. M. and Oerlemans, J.: Simulated future sea-level rise due to glacier melt based on regionally and seasonally resolved temperature changes, Nature, 391, 474–476, https://doi.org/10.1038/35119, 1998.

Hammes, K., Schmidt, M. W. I., Smernik, R. J., Currie, L. A., Ball, W. P., Nguyen, T. H., Louchouarn, P., Houel, S., Gustafsson, Ö., Elmquist, M., Cornelissen, G., Skjemstad, J. O., Masiello, C. A., Song, J., Peng, P., Mitra, S., Dunn, J. C., Hatcher, P. G., Hockaday, W. C., Smith, D. M., Hartkopf-Fröder, C., Böhmer, A., Lüer, B., Huebert, B. J., Amelung,W., Brodowski, S., Huang, L., Zhang, W., Gschwend, P. M., Flores-Cervantes, D. X., Largeau, C., Rouzaud, J., Rumpel, C., Guggenberger, G., Kaiser, K., Rodionov, A., Gonzalez-Vila, F. J., Gonzalez-Perez, J. A., de la Rosa, J. M., Manning, D. A. C., López-Capél, E., and Ding, L.:, Comparison of quantification methods to measure fire-derived (black/elemental) carbon in soils and sediments using reference materials from soil, water, sediment and the atmosphere, Global Biogeochem. Cy., 21, GB3016, https://doi.org/10.1029/2006GB002914, 2007.

Hansen, J. and Nazarenko, L.: Soot climate forcing via snow and ice albedos, P. Natl. Acad. Sci. USA, 101, 423–428, https://doi.org/10.1073/pnas.2237157100, 2004.

Hill, A. F., Rittger, K., Dendup, T., Tshering, D., and Painter, T. H.: How important is meltwater to the Chamkhar Chhu headwaters of the Brahmaputra River?, Front. Earth Sci., 8, 81, https://doi.org/10.3389/feart.2020.00081, 2020.

Immerzeel, W. W., van Beek, L. P. H., and Bioerkens, M. F. P.: Climate change will affect the Asian water towers, Science, 328, 1382–1385, https://doi.org/10.1126/science.1183188, 2010.

IPCC: Climate Change 2013: The Physical Science Basis, Contribution of Working Group I to the Fifth Assessment Report of the Intergovernmental Panel on Climate Change, edited by: Stocker, T. F., D. Qin, G.-K. Plattner, M. Tignor, S. K. Allen, J. Boschung, A. Nauels, Y. Xia, V. Bex, and P. M. Midgley, Cambridge University Press, Cambridge, United Kingdom and New York, NY, USA, 1535 pp., https://doi.org/10.1017/CBO9781107415324, 2013.

Jacobson, M. Z.: Climate response of fossil fuel and biofuel soot, accounting for soot's feedback to snow and sea ice albedo and emissivity, J. Geophys. Res., 109, D21201, https://doi.org/10.1029/2004JD004945, 2004.

Jenkins, M., Kaspari, S., Kang, S.-C., Grigholm, B., and Mayewski, P. A.: Tibetan Plateau Geladaindong black carbon ice core record (1843-1982): Recent increases due to higher emissions and lower snow accumulation, Adv. Clim. Change Res., 7, 132–138, https://doi.org/10.1016/j.accre.2016.07.002, 2016.

Kaspari, S. D., Schwikowski, M., Gysel, M., Flanner, M. G., Kang, S., Hou, S., and Mayewski, P. A.: Recent increase in black carbon concentrations from a Mt. Everest ice core spanning 1860–2000 AD, Geophys. Res. Lett., 38, L04703, https://doi.org/10.1029/2010GL046096, 2011.

Kaspari, S., Painter, T. H., Gysel, M., Skiles, S. M., and Schwikowski, M.: Seasonal and elevational variations of black carbon and dust in snow and ice in the Solu-Khumbu, Nepal and estimated radiative forcings, Atmos. Chem. Phys., 14, 8089–8103, https://doi.org/10.5194/acp-14-8089-2014, 2014.

Kopacz, M., Mauzerall, D. L., Wang, J., Leibensperger, E. M., Henze, D. K., and Singh, K.: Origin and radiative forcing of black carbon transported to the Himalayas and Tibetan Plateau, Atmos. Chem. Phys., 11, 2837–2852, https://doi.org/10.5194/acp-11-2837-2011, 2011.

Kumar, R., Barth, M. C., Pfister, G. G., Nair, V. S., Ghude, S. D., and Ojha, N.: What controls the seasonal cycle of black carbon aerosols in India?, J. Geophys. Res.-Atmos., 120, 7788-7812, https://doi.org/10.1002/2015JD023298, 2015.

Lack, D. A., Moosmüller, H., McMeeking, G. R., Chakrabarty, R. K., and Baumgardner, D.: Characterizing elemental, equivalent black, and refractory black carbon aerosol particles: a review of techniques, their limitations and uncertainties, Anal. Bioanal. Chem., 406, 99–122, https://doi.org/10.1007/s00216-013-7402-3, 2014.

Lau, W. K. M. and Kim, K. M.: Fingerprinting the impacts of aerosols on long-term trends of the Indian summer monsoon regional rainfall, Geophys. Res. Lett., 37, L16705, https://doi.org/10.1029/2010GL043255, 2010.

Lee, Y. H., Lamarque, J.-F., Flanner, M. G., Jiao, C., Shindell, D. T., Berntsen, T., Bisiaux, M. M., Cao, J., Collins, W. J., Curran, M., Edwards, R., Faluvegi, G., Ghan, S., Horowitz, L. W., McConnell, J. R., Ming, J., Myhre, G., Nagashima, T., Naik, V., Rumbold, S. T., Skeie, R. B., Sudo, K., Takemura, T., Thevenon, F., Xu, B., and Yoon, J.-H.: Evaluation of preindustrial to present-day black carbon and its albedo forcing from Atmospheric Chemistry and Climate Model Intercomparison Project (ACCMIP), Atmos. Chem. Phys., 13, 2607–2634, https://doi.org/10.5194/acp-13-2607-2013, 2013.

Lelieveld, J., Bourtsoukidis, E., Bruhl, C., Fischer, H., Fuchs, H., Harder, H., Hofzumahaus, A., Holland, F., Marno, D., Neumaier, M., Pozzer, A., Schlager, H., Williams, J., Zahn, A., and Ziereis, H.: The South Asian monsoon – pollution pump and purifier, Science, 361, 270–273, https://doi.org/10.1126/science.aar2501, 2018.

Li, S., Yao, T., Tian, L., and Wang, P.: Seasonal transition characteristics of the westerly jet: Study based on field observations at an altitude of 6900 m on the Mt. Xixiabangma Dasuopu glacier, Chinese Sci. Bull., 56, 1912–1920, https://doi.org/10.1007/s11434-011-4508-x, 2011.

Lindberg, J. D., Douglass, R. E., and Garvey, D. M.: Atmospheric particulate absorption and black carbon measurement, Appl. Optics, 38, 2369–2376, https://doi.org/10.1364/AO.38.002369, 1999.

Liu, X., Xu, B., Yao, T., Wang, N., and Wu, G.: Carbonaceous particles in Muztagh Ata ice core, west Kunlun mountains, China, Chinese Sci. Bull., 53, 3379–3386, https://doi.org/10.1007/s11434-008-0294-5, 2008.

Lund, M. T., Samset, B. H., Skeie, R. B., Watson-Parris, D., Katich, J. M., Schwarz, J. P., and Weinzierl, B.: Short black carbon lifetime inferred from a global set of aircraft observations, NPJ Climate and Atmospheric Science, 1, 31, https://doi.org/10.1038/s41612-018-0040-x, 2018.

Marinoni, A., Cristofanelli, P., Laj, P., Duchi, R., Calzolari, F., Decesari, S., Sellegri, K., Vuillermoz, E., Verza, G. P., Villani, P., and Bonasoni, P.: Aerosol mass and black carbon concentrations, a two year record at NCO-P (5079 m, Southern Himalayas), Atmos. Chem. Phys., 10, 8551–8562, https://doi.org/10.5194/acp-10-8551-2010, 2010.

Marinoni, A., Cristofanelli, P., Laj, P., Duchi, R., Putero, D, Calzolari, F., Landi, T. C., Vuillermoz, E., Maione, M., and Bonasoni, P.: High black carbon and ozone concentrations during pollution transport in the Himalayas: five years of continuous observations at NCO-P global GAW station, J. Environ. Sci. (China), 25, 1618–1625, https://doi.org/10.1016/S1001-0742(12)60242-3, 2013.

Menking, J. A.: Black carbon measurement of snow and ice using the single particle soot photometer: Method development and an AD 1852-1999 record of atmospheric black carbon from a Mount Logan ice core. MS thesis, Central Washington University, Ellensburg, WA, https://digitalcommons.cwu.edu/etd/1447 (last access: 7 April 2021), 2013.

Ming, J., Cachier, H., Xiao, C., Qin, D., Kang, S., Hou, S., and Xu, J.: Black carbon record based on a shallow Himalayan ice core and its climatic implications, Atmos. Chem. Phys., 8, 1343–1352, https://doi.org/10.5194/acp-8-1343-2008, 2008.

Ming, J., Du, Z., Xiao, C., Xu, X., and Zhang, D.: Darkening of the mid-Himalaya glaciers since 2000 and the potential causes, Environ. Res. Lett., 7, 014021, https://doi.org/10.1088/1748-9326/7/1/014021, 2012.

Mishra, V., Tiwari, A. D., Aadhar, S., Shah, R., Xiao, M., Pai, D. S., and Lettenmaier, D.: Drought and famine in India, 1870–2016, Geophys. Res. Lett., 46, 2075–2083, https://doi.org/10.1029/2018GL081477, 2019.

Montanari, L., Basu, B., Spagnoli, A., and Broderick, B. M.: A padding method to reduce edge effects for enhanced damage identification using wavelet analysis, Mech. Syst. Signal Pr., 52–52, 264–277, https://doi.org/10.1016/j.ymssp.2014.06.014, 2015.

Mooley, D. A., Parthasarathy, B., Sontakke, N. A., and Munot, A. A.: Annual rain-water over India, its variability and impact on the economy, J. Climatol., 1, 167–186, https://doi.org/10.1002/joc.3370010206, 1981.

Nair, V. S., Babu, S. S., Moorthy, K. K., Sharma, A. K., Marinoni, A., and Ayai: Black carbon aerosols over the Himalayas: direct and surface albedo forcing, Tellus B, 65, 1–14, https://doi.org/10.3402/tellusb.v65i0.19738, 2013.

Negi, P. S., Pandey, C. P., and Singh, N.: Black carbon aerosol in the ambient air of Gangotri Glacier valley of northwestern Himalaya in India, Atmos. Environ., 214, 116879, https://doi.org/10.1016/j.atmosenv.2019.116879, 2019.

Niu, H., Kang, S., Shi, X., Paudyal, R., He, Y., Li, G., Wang, S., Pu, T., and Shi, X.: In-situ measurements of light-absorbing imputities in snow of glacier on Mt. Yulong and implications for radiative forcing estimates, Sci. Total Environ., 581–582, 848–856, https://doi.org/10.1016/j.scitotenv.2017.01.032, 2017.

Novakov, T., Ramanathan, V., Hansen, J. E., Kirchstetter, T. W., Sato, M., Sinton, J. E., and Sathaye, J. A., Large historical changes of fossil-fuel black carbon aerosols, Geophys. Res. Lett., 30, 1324, https://doi.org/10.1029/2002GL016345, 2003.

Ogren, J. A., and Charlson, R. J.: Elemental carbon in the atmosphere: cycle and lifetime, Tellus B, 35, 241–254, https://doi.org/10.1111/j.1600-0889.1983.tb00027.x, 1983.

Parthasarathy, B., Sontakke, N. A., Monot, A. A., and Kothawale, D. R.: Droughts/floods in the summer monsoon season over different meteorological subdivisions of India for the period 1871–1984, Int. J. Climatol., 7, 57–70, https://doi.org/10.1002/joc.3370070106, 1987.

Petzold, A., Ogren, J. A., Fiebig, M., Laj, P., Li, S.-M., Baltensperger, U., Holzer-Popp, T., Kinne, S., Pappalardo, G., Sugimoto, N., Wehrli, C., Wiedensohler, A., and Zhang, X.-Y.: Recommendations for reporting "black carbon" measurements, Atmos. Chem. Phys., 13, 8365–8379, https://doi.org/10.5194/acp-13-8365-2013, 2013.

Rahaman, W., Chatterjee, S., Ejaz, T., and Thamban, M.: Increased influence of ENSO on Antarctic temperature since the Industrial Era, Sci. Rep.-UK, 9, 6006, https://doi.org/10.1038/s41598-019-42499-x, 2019.

Ramanathan, V. and Carmichael, G.: Global and regional climate changes due to black carbon, Nat. Geosci., 1, 221–227, https://doi.org/10.1038/ngeo156, 2008.

Ramanathan, V., Ramana, M. V., Roberts, G., Kim, D., Corrigan, C., Chung, C., and Winker, D.: Warming trends in Asia amplified by brown cloud solar absorption, Nature, 448, 575–578, https://doi.org/10.1038/nature06019, 2007.

Raper, S. C. B. and Braithwaite, R. J.: Low sea level rise projections from mountain glaciers and icecaps under global warming, Nature, 439, 311–313, https://doi.org/10.1038/nature04448, 2006.

Reddy, M. S. and Boucher, O.: A study of the global cycle of carbonaceous aerosols in the LMDZT general circulation model, J. Geophys. Res., 109, D14202, https://doi.org/10.1029/2003JD004048, 2004.

Reddy, M. S. and Boucher, O.: Climate impact of black carbon emitted from energy consumption in the world's regions, Geophys. Res. Let., 34, L11802, https://doi.org/10.1029/2006GL028904, 2007.

Ross, A. B., Jones, J. M., Chaiklangmuang, S., Pourkashanian, M., Williams, A., Kubica, K., Andersson, J. T., Kerst, M., Danihelka, P., and Bartle, K. D.: Measurement and prediction of the emission of pollutants from the combustion of coa and biomass in a fixed bed furnace, Fuel, 81, 571–582, https://doi.org/10.1016/S0016-2361(01)00157-0, 2002.

Samset, B. H., Myhre, G., Herber, A., Kondo, Y., Li, S.-M., Moteki, N., Koike, M., Oshima, N., Schwarz, J. P., Balkanski, Y., Bauer, S. E., Bellouin, N., Berntsen, T. K., Bian, H., Chin, M., Diehl, T., Easter, R. C., Ghan, S. J., Iversen, T., Kirkevåg, A., Lamarque, J.-F., Lin, G., Liu, X., Penner, J. E., Schulz, M., Seland, Ø., Skeie, R. B., Stier, P., Takemura, T., Tsigaridis, K., and Zhang, K.: Modelled black carbon radiative forcing and atmospheric lifetime in AeroCom Phase II constrained by aircraft observations, Atmos. Chem. Phys., 14, 12465–12477, https://doi.org/10.5194/acp-14-12465-2014, 2014.

Samsonov, Y. N., Ivanov, V. A., McRae, D. J., and Baker, S. P.: Chemical and dispersal characteristics of particulate emissions from forest fires in Siberia, Int. J. Wildland Fire, 21, 818–827, https://doi.org/10.1071/WF11038, 2012.

Schwarz, J. P., Gao, R. S., Fahey, D. W., Thomson, D. S., Watts, L. A., Wilson, J. C., Reeves, J. M., Darbeheshti, M., Baumgardner, D. G., Kok, G. L., Chung, S. H., Schulz, M., Hendricks, J., Lauer, A., Karcher, B., Slowik, J. G., Rosenlof, K. H., Thompson, T. L., Langford, A. O., Loewenstein, M., and Aikin, K. C.: Single-particle measurements of midlatitude black carbon and light-scattering aerosols from the boundary layer to the lower stratosphere, J. Geophys. Res.-Atmos., 111, D16207, https://doi.org/10.1029/2006JD007076, 2006.

Scott, C. A., Zhang, F., Mukherji, A., Immerzeel, W., Mustafa, D., and Bharati, L.: Water in the Hindu Kush Himalaya, in: The Hindu Kush Himalaya Assessment, edited by: Wester, P., Mishra, A., and Shrestha, A., Springer, Cham, https://doi.org/10.1007/978-3-319-92288-1_8, 2019.

Solanki, R. and Singh, N.: LiDAR observations of the vertical distribution of aerosols in free troposphere: Comparison with CALIPSO level-2 data over central Himalayas, Atmos. Environ., 99, 227–238, https://doi.org/10.1016/j.atmosenv.2014.09.083, 2014.

Stothers, R. B.: The great Tambora eruption in 1815 and its aftermath, Science, 224, 1191–1198, https://doi.org/10.1126/science.224.4654.1191, 1984.

Su, H., Liu, Q., and Li, J.: Alleviating border effects in wavelet transforms for nonlinear time-varying signal analysis, Adv. Electr. Comput. En., 11, 55–60, https://doi.org/10.4316/AECE.2011.03009, 2011.

Thapa, U. K., St. George, S., Kharal, D. K., and Gaire, N. P.: Tree growth across the Nepal Himalaya during the last four centuries, Prog. Phys. Geog., 41, 478–495, https://doi.org/10.1177/0309133317714247, 2017.

Thind, P. S., Chandel, K. K., Sharma, S. K., Mandal, T. K., and John, S.: Light-absorbing impurities in snow of the Indian Western Himalayas: impact on snow albedo, radiative forcing, and enhanced melting, Environ. Sci. Pollut. R., 26, 7566–7578, https://doi.org/10.1007/S11356-019-04183-5, 2019.

Thompson, L. G., Yao, T., Mosley-Thompson, E., Davis, M. E., Henderson, K. A., and Lin, P.-N.: A high-resolution millennial record of the south Asian monsoon from Himalayan ice cores, Science, 289, 1916–1919, https://doi.org/10.1126/science.289.5486.1916, 2000.

Torrence, C. and Compo, G. P.: A practical guide to wavelet analysis, Bull. Am. Meteorol. Soc., 79, 61–78, https://doi.org/10.1175/1520-0477(1998)079<0061:APGTWA>2.0.CO;2, 1998.

Tosca, M. G., Randerson, J. T., Zender, C. S., Flanner, M. G., and Rasch, P. J.: Do biomass burning aerosols intensify drought in equatorial Asia during El Niño?, Atmos. Chem. Phys., 10, 3515–3528, https://doi.org/10.5194/acp-10-3515-2010, 2010.

Uglietti, C., Gabrielli, P., Olesik, J. W., Lutton, A., and Thompson, L. G.: Laerge variability of trace element mass fractions determined by ICP-SFMS in ice core samples from worldwide high altitude glaciers, Appl. Geochem., 47, 109–121, https://doi.org/10.1016/j.apgeochem.2014.05.019, 2014.

Wang, M., Xu, B., Kaspari, S. D., Gleixner, G., Schwab, V. F., Zhao, H., Wang, H., and Yao, P.: Century-long record of black carbon in an ice core from the Eastern Pamirs: Estimated contributions from biomass burning, Atmos. Environ., 115, 79–88, https://doi.org/10.1016/j.atmosenv.2015.05.034, 2015.

Wendl, I. A., Menking, J. A., Färber, R., Gysel, M., Kaspari, S. D., Laborde, M. J. G., and Schwikowski, M.: Optimized method for black carbon analysis in ice and snow using the Single Particle Soot Photometer, Atmos. Meas. Tech., 7, 2667–2681, https://doi.org/10.5194/amt-7-2667-2014, 2014.

Xu, B., Cao, J., Hansen, J., Yao, T., Joswia, D. R., Wang, N., Wu, G., Wang, M., Zhao, H., Yang, W., Liu, X., and He, J.: Black soot and the survival of Tibetan glaciers, P. Natl. Acad. Sci. USA, 106, 22114–22118, https://doi.org/10.1073/pnas.0910444106, 2009.

Xu, B., Cao, J., Joswiak, D. R., Liu, X., Zhao, H., and He, J.: Post-depositional enrichment of black soot in snow-pack and accelerated melting of Tibetan glaciers, Environ. Res. Lett., 7, 014022, https://doi.org/10.1088/1748-9326/7/1/014022, 2012.

Yang, M., Yao, T., Wang, H., and Gou, X.: Climatic oscillations over the past 120 kyr recorded in the Guliya ice core, China, Quatern. Int., 154-155, 11–18, https://doi.org/10.1016/j.quaint.2006.02.015, 2006.

Zhang, Y., Kang, S., Sprenger, M., Cong, Z., Gao, T., Li, C., Tao, S., Li, X., Zhong, X., Xu, M., Meng, W., Neupane, B., Qin, X., and Sillanpää, M.: Black carbon and mineral dust in snow cover on the Tibetan Plateau, The Cryosphere, 12, 413–431, https://doi.org/10.5194/tc-12-413-2018, 2018.